5-2017

Applications of Side Scan and Parametric Echosounders for Mapping Shallow Seagrass Habitats and Their Associated Organic Carbon

Austin L. Greene
The University of Texas Rio Grande Valley

APPLICATIONS OF SIDE SCAN AND PARAMETRIC ECHOSOUNDERS FOR MAPPING SHALLOW SEAGRASS HABITATS AND THEIR ASSOCIATED ORGANIC CARBON

A Thesis

by

AUSTIN L. GREENE

Submitted to the Graduate College of
The University of Texas Rio Grande Valley
In partial fulfillment of the requirements for the degree of

MASTER OF SCIENCE

May 2017

Major Subject: Biology

APPLICATIONS OF SIDE SCAN AND PARAMETRIC ECHOSOUNDERS FOR MAPPING SHALLOW SEAGRASS HABITATS AND THEIR ASSOCIATED ORGANIC CARBON

A Thesis
by
AUSTIN L. GREENE

COMMITTEE MEMBERS

Dr. Abdullah Rahman
Chair of Committee

Dr. Richard Kline
Committee Member

Dr. Preston Wilson
Committee Member

Dr. Kenneth Dunton
Committee Member

Dr. M.D Saydur Rahman
Committee Member

May 2017

ABSTRACT

Greene, Austin L., Applications of Side Scan and Parametric Echosounders for Mapping Shallow Seagrass Habitats and Their Associated Organic Carbon. Master of Science (MS), May, 2017, 101 pp, 1 table, 35 figures, references 75 titles.

Despite a global valuation of $1.9 trillion seagrass habitats world-wide are in decline - directly impacting the large soil carbon stocks associated with seagrasses. Many methods exist to measure the health of seagrass habitats, yet few apply to shallow coastal ecosystems. Those that do lack spatial resolution (satellite surveys) or do not provide continuous data across large areas (point-based surveys). Furthermore, carbon content of these ecosystems is largely limited to destructive and time-consuming soil core sampling. Side scan and parametric acoustics represent a unique technological opportunity to study habitat coverage and carbon content of vegetated coastal habitats (< 3 m depth). This study presents proof of concept for applications of recreational side scan and parametric sub-bottom profiling sonars in mapping both habitat coverage and organic carbon distribution in shallow seagrass habitats, and explores how these methods might be improved in future applications.

DEDICATION

To my family and loved ones for supporting me and to my mentors for inspiring me.

ACKNOWLEDGMENTS

I will always be grateful to my committee chair and advisor Dr. Abdullah Rahman for his insight and motivation throughout this process. My thanks also go to all those who helped me in my field work or data processing, especially my lab mates Aslan Aslan and Stephanie DuBois. Aslan and Stephanie's willingness to endure incredibly long field days and help me in my surveying is what made this work possible. I would also like to thank the Digital Globe Foundation for donating the satellite imagery utilized in the side scan chapter of this work. To all others who helped me from UTRGV, the UTRGV Coastal Studies Lab, UT Austin, and abroad – thank you.

TABLE OF CONTENTS

LIST OF TABLES

Page

LIST OF FIGURES

Page

CHAPTER I

INTRODUCTION

Statement of Problem

Seagrasses as submerged aquatic vegetation (SAV) are a critical component of shallow coastal ecosystems and provide a multitude of ecosystem services. Seagrass meadows are highly productive (McRoy & McMillan, 1977), act as a food or habitat source for many aquatic species (Lee & Dunton, 1996), limit erosion (Bos et al., 2007), and contribute up to 15% of global ocean carbon sequestration (Fourqurean et al., 2012). Despite recognition as an indicator for the health of coastal ecosystems (Dekker et al., 2003) SAV habitats are experiencing global decline, threatening more than $1.9 trillion in associated ecosystem services (Waycott et al., 2009). Declining seagrass cover has been associated with anthropogenic pressures, increasing surface temperatures, and rising sea levels (Pergent et al., 2014). In the face of mounting losses, robust and accurate methods for mapping seagrass habitat coverage and the carbon-rich sediments associated with these areas are critical to understanding the impacts of seagrass habitat loss (Luo et al., 2016).

Labeled as “coastal canaries” for their role as indicators of ecosystem health (Orth et al., 2006), seagrass meadows frequently become fragmented in shallow waters where anthropogenic pressures such as vessel scarring are high (Uhrin & Holmquist, 2003). Fragmentation of habitats and increasing edge-effects have been linked to reductions in biodiversity (Wilcox & Murphy,

1985 ; Majer et al., 1997). Effects of physical disturbances on seagrass habitats such as propeller scarring have been shown to represent an immediate loss of plant matter lasting up to seven years, a prolonged loss of extractable ammonium, and a significant loss of organic matter (Dawes et al, 1997). Fragmentation in seagrass beds has also been linked to a significant reduction in macrofaunal abundance extending up to 5 m into meadows which adjoin a disturbed area (Uhrin & Holmquist, 2003). Exposure of sediments within seagrass beds can also lead to increased sediment resuspension and turbidity, reducing the ability of seagrasses to photosynthesize (Dunton & Schonberg, 2002). The fragmented nature of increasingly disturbed seagrass meadows represents a significant challenge to mapping efforts required for the successful management of these valuable habitats.

Carbon characteristics of seagrass-associated soils are similarly cryptic and difficult to survey. Despite sequestering more carbon than tropical, boreal, or temperate forests (McLeod et al., 2011), methods for the study of seagrass carbon sequestration have not appreciably advanced beyond the collection of destructive and labor-intensive soil cores. Traditional sub-bottom profiling sonars and echosounders are largely ineffective in seagrass meadows due to attenuative and scattering effects of the plant's arenchynous gas-exchange tissues (Wilson & Dunton, 2009). Seagrass-associated sediments are similarly gaseous and present yet another hurdle to sub-bottom sonar surveys (Wilson et al., 2007 ; Wilson et al.,, 2008). Recent advancements in sonar technology allow the use of low-frequency high-resolution parametric waves to better survey sub-bottom layers. Parametric waves feature reduced side lobes, allowing improved resolution and reduced noise which may aid in detecting layers beneath seagrass-associated sediments. Parametric sonars have been used to estimate carbon content in simple systems of matte-forming seagrasses by estimating total detritus matte volume and extrapolating from soil core data on

carbon content (Lo Iacono et al., 2008). The work of Lo Iacono et al. (2008) also occurred in water depths greater than those of many shallow seagrasses ecosystems (4 m+) which may influence parametric performance. Parametric capabilities have not been demonstrated in the complex systems of common, non-matte-forming seagrasses wherein organic carbon is deposited directly into a continuous soil matrix. The ability to remotely estimate carbon content within a continuous seagrass soil matrix would provide a valuable tool to the study of carbon pools in coastal habitats and encourage efficient, large-scale study of these systems with only a limited number of soil cores for data validation.

Thesis Objectives

Side scan - Chapter 1: Use commercially available components to construct a single-beam side scan sonar system that is inexpensive, easily deployable, and capable of accurately mapping seagrass beds with high resolution imagery in very shallow conditions. The primary objective of this research is to test whether SSS can be used as an effective tool for mapping and monitoring of seagrass meadows occurring in shallow coastal regions with a depth of approximately 1 m. The secondary objective of this chapter is to quantify the primary sources of error in the proposed system by measuring across-track and along-track distortions *in situ*, and to compare the performance of SSS in very shallow macrophyte beds to that of both satellite and aerial imagery resources commonly used to survey these habitats.

Parametric - Chapter 2: Leverage recent advancements and availability of parametric echosounders to determine if these technologies can reliably detect seabed layering in seagrass meadows. Laboratory testing will determine if parametric sonar can detect fine sediment layers in a controlled setting under ideal conditions. Field testing in a living seagrass meadow will test if parametric sonar can detect discrete layers in a complex soil matrix. Parametric results will be

compared to soil core characteristics collected from the study site. If possible, parametric results and soil characteristics will be combined to provide insights into the distribution and quantity of organic carbon across a living seagrass meadow. Satisfactory completion of these objectives will provide further proof-of-concept of new methods to remotely estimate carbon pools in seagrass meadows and encourage further development for the continuous modeling of organic carbon distributions in shallow, coastal ecosystems.

Study Site

A large study site approximately 88,000 m^2 was chosen from within the Lower Laguna Madre (LLM), a highly disturbed, mixed-bed seagrass habitat in southern Texas near South Padre Island (Fig. 1). The site was chosen based on its varying seagrass cover, presence of empty patches, high anthropogenic disturbance, and easy access. The selected site was utilized for both side scan and parametric sonar components of this study.

The LLM contains 80% of all remaining seagrass habitat in Texas (Blankenship, 2006), provides wintering habitat for 77% of all North American Redhead ducks, and sustains several industries as Texas' most productive bay fishery (Tunnell & Judd, 2002). The site was dominated by *Thalassia testudinum* and featured bare patches in a variety of sizes ranging from less than 1 m^2 to greater than 85 m^2. Bottom substrate ranged from soft sediments in seagrass meadows to firm sand in bare patches while depths for the entire LLM average just 75 cm (Quammen and Onuf, 1993).

For the side scan component, drone imagery and six side scan transects were collected from a smaller region (~ 88,000 m^2, Fig. 1 Panel 3) within the test site and used in concert with high-resolution satellite imagery to meet chapter 1 objectives. To meet objectives of the parametric component, a total of 26 continuous parametric transects, 23 stationary parametric

recordings, and 23 sediment cores were also collected from a region approximating 52,000 m^2 from within the study site.

Figure 1, aerial imagery of the study site - all side scan and parametric surveys were conducted in the Lower Laguna Madre in a disturbed seagrass meadow near South Padre Island.

CHAPTER II

USE OF A RECREATIONAL SIDE SCAN SONAR FOR HIGH-RESOLUTION MAPPING OF SHALLOW SEAGRASS HABITATS

Abstract

Worldwide, seagrass beds are in decline. Studies have shown that global seagrass habitat is lost at a rate of 110 km^2 per year, resulting in a 29% loss since 1879. With 7% of all seagrass disappearing each year, the $1.9 trillion of nutrient cycling service associated with these habitats is also in jeopardy (Waycott et al., 2009). Cost, logistical complexity, and resolution can vary greatly across the many available methods for surveying seagrass meadows. Optical surveys are limited by turbidity, cloud cover, and water reflectance. Traditional acoustic methods have demonstrated utility for mapping macrophytes in deeper regions (> 6 m), but suffer from limited swath width in shallow regions (< 3 m) typical of many seagrass meadows. The use of consumer-grade side scan sonar (SSS) provides a low-cost method capable of collecting high-resolution imagery in shallow environments, and is unaffected by turbidity or meteorological conditions. In this study, we demonstrate the deployment of an SSS array in a 60,000 m^2 test plot of shallow seagrass meadow and compare SSS measurements of habitat structure to those collected with satellite and aerial photography.

Introduction

Seagrass Habitat

Seagrasses as submerged aquatic vegetation (SAV) are a critical component of shallow coastal ecosystems and provide a multitude of ecosystem services. Seagrass meadows are highly productive (McRoy & McMillan, 1977), act as a food or habitat source for many aquatic species (Lee & Dunton, 1996), limit erosion (Bos et al., 2007), and contribute up to 15% of global ocean carbon sequestration (Fourqurean et al., 2012). Despite recognition as an indicator for the health of coastal ecosystems (Dekker et al., 2003) SAV habitats are experiencing global decline, threatening more than $1.9 trillion in associated ecosystem services (Waycott et al., 2009). Declining of seagrass cover has been associated with anthropogenic pressures, increasing surface temperatures, rising sea levels, and even competition with less-robust SAV associated with warmer climates (Pergent et al., 2014). In the face of mounting losses, robust and accurate methods for mapping seagrass coverage are critical to understanding the spatial extent of seagrass habitat loss and its associated impacts (Luo et al., 2016).

Labeled as "coastal canaries" for their role as indicators of ecosystem health (Orth et al., 2006), seagrass meadows frequently become fragmented in shallow waters where anthropogenic pressures are high (Uhrin & Holmquist, 2003). Fragmentation of habitats and increasing edge-effects have been thoroughly linked to reductions in biodiversity (Wilcox & Murphy, 1985 ; Majer et al., 1997). While fragmentation in marine habitats has experienced limited study, the effects of physical disturbances on seagrass habitats such as propeller scarring has been shown to represent an immediate loss of plant matter lasting up to seven years, a prolonged loss of extractable ammonium, and a loss of organic matter (Dawes et al., 1997). Fragmentation in seagrass beds has also been linked to a significant reduction in macrofaunal abundance extending

up to 5 m into meadows which adjoin a disturbed area (Uhrin & Holmquist, 2003). Exposure of sediments within seagrass beds can also lead to increased sediment resuspension and turbidity, reducing the ability of seagrasses to photosynthesize (Dunton & Schonberg, 2002). The fragmented nature of increasingly disturbed seagrass meadows represents a significant challenge to mapping efforts required for the successful management of these valuable habitats.

Current Mapping Methods

Many tools exist for mapping seagrass coverage including aerial photographs (Dunton & Schonberg, 2002), satellite imagery (Phinn et al., 2008), rapid visual sampling (Fourqurean et al., 2001), acoustic doppler current profilers (ADCP) (Warren & Peterson, 2007), multi-beam sonar (MBS) (Komatsu et al., 2003), single-beam sediment profilers (Lefebvre et al., 2009), single-beam sonar (Riegl et al., 2005), parametric sonar (Lo Iacono et al., 2008), side scan sonar (Lucieer, 2008), and underwater videography (Norris et al., 1997). There exists no standard method for mapping seagrass systems, and methods vary greatly in cost and resolution. Researchers often select a technique based on many factors such as weather, sea conditions, turbidity, desired spatial and temporal resolution, instrument availability, required manpower, and cost. Acoustic methods have been widely utilized for mapping macrophyte cover at depths greater than 6 m. However, studies of mapping very shallow seagrass meadows are lacking in the literature despite habitats at depths of 1 m or less being at increased risk of physical disturbance (Zieman, 1976). This could be due in part to the limited acoustic methods for studying very shallow habitats.

Satellite imagery represents a comparatively low-resolution alternative to the expensive practice of aerial photography, instead covering large areas with low detail (Mumby et al., 1999). Common satellites used for SAV surveys include MODIS, IKONOS, and WorldView which

offer resolutions of 250 m/px, 0.82 m/px, and 0.30 m/px, respectively. However, these resolutions may not be sufficient to clearly discern the small bare patches which occur in seagrass meadows, or discriminate algae-filled bare patches from the surrounding macrophyte cover. Aerial imagery captured via fixed-wing aircraft offers increased resolution (0.15 m/px) and logistical flexibility at a greatly increased cost. Recent availability of remote controlled drone aircraft has provided a low-cost alternative to traditional aerial surveys. While offering a high-resolution alternative (4.5 cm/px in this study), drone surveys may require significant post-processing, and recently have come under legislative restriction (FAA). Satellite imagery, fixed-wing aerial photography, and drone surveys are all heavily impacted by cloud cover, high reflectivity of the water surface, and high turbidity. Other survey methods commonly employed include towed video transects (Norris et al., 1997) and point-based rapid visual sampling (Fourqurean et al., 2001). Video transects provide continuous real-time data on the seagrass habitat, but cannot function in high turbidity. Rapid visual sampling has proven a promising method for quickly mapping large areas, yet inherently requires statistical inference between sample points and does not provide continuous data on seagrass coverage.

Hydroacoustic methods such as single or multi beam echosounders are unaffected by high turbidity and allow surveying under a wide range of environmental conditions. Multi-beam echosounders appear most frequently in the literature due to their ability to simultaneously measure canopy height, approximate shoot density, infer species composition, and collect limited bathymetrics. Hamana & Komatsu (2016) demonstrated the use of multibeam sonar in characterizing seagrass beds which occur over a sandy bottom, yet did not demonstrate these applications in conditions shallower than 6 m. Bucas et al., (2016) has shown promising use of low-cost, bottom-facing recreational fishing sonars for discriminating charophyte and

angiosperm presence on the seafloor, but also did not find significant results at depths shallower than 1 m or where algal cover was high. Bucas et al., (2016) also reported that while SSS data was collected in their study, the shallow depth of survey areas limited horizontal swath and therefore utility. SSS has a rich history of being used to classify seagrass cover in deeper meadows (Pasquialini et al., 1998 ; Pasquialini et al., 2000, ; Ardizzone et al., 2006, ; Sanchez-Carnero et al., 2012), yet little evidence in the literature indicates quantitative study of these methods or their inherent distortions in shallow (< 3 m) seagrass beds.

To date much side scan research conducted in seagrass has been the product of military mine-hunting feasibility studies. These studies have found that side scan may represent seagrass coverage as well as aerial photos, and may be largely unaffected by algal cover (Mulhearn, 2001). One study in shallow river systems showed promise in feature identification by using a recreational side scan transducer (Kaeser & Litts, 2011). Theoretical studies of side scan distortions exist, yet the authors could not locate any studies which quantify the dominant effects of distortions on measurements of real-world habitat features (ex: bare patches) in shallow seagrass beds. An exploration of this topic is critical when attempting to accurately map habitat disturbance or heterogeneity in shallow seagrass beds.

Suitability of Side Scan for Mapping Seagrass Habitats

Echosounders function on the basic property of insonifying a swath of seabed and receiving “returns” as reflections of the outgoing wave as it interacts with the seabed (Kenny et al., 2003). Both frequency, pulse duration, and horizontal band width influence the overall resolution a given wave can produce. High frequency waves can resolve smaller objects but suffer from a reduced horizontal range. Low frequency waves may only resolve larger objects, but feature increased range. The distance to a target object can be calculated based on the time

between when a ping is generated and when reflection pings are received. By compiling returns as a transducer moves along a known path, an image of the surrounding environment may be constructed one ping, or set of pings at a time.

Multi-beam echosounders function by using an array of transducers at preconfigured angles and sending pings downward into the water column (Gerlotto et al., 1999). At any given time, these transducers function simultaneously to produce a "slice", or vertical cross-section, which can then be combined over time to form an image. Basic side scan echosounders are typically towed behind a vessel, utilize two transducers (one port, one starboard), and send out successive, horizontal pings as the towfish is pulled along a path. Returns from these pings are rectified with bathymetric data to form an image line-by-line, mapping all features perpendicular to the direction of travel (Fig. 2). Side scan echosounder transducers are configured at shallow horizontal angles and thus perform best when close to the seafloor. Multibeam horizontal range is limited by a steep bathymetry beam angle - SSS does not share this limitation and can provide far greater effective range (Le Bas & Huvenne 2009).

SSS holds several advantages over traditional satellite, aerial, or random visual field sampling methods for mapping seagrass habitats. Unlike aerial or satellite images, SSS is largely unaffected by turbidity, and can produce high-resolution imagery (2.54 cm/px) in murky water (Pasqualini et al., 1999). Side scan is also capable of observing macrophyte beds in lower photic regions too deep for optical methods (Karpouzli & Malthus 2007). Unlike satellite or aerial imagery, cloud-cover, reflected sunlight, and atmospheric distortions do not inhibit sonar. Under these sub-optimal surveying conditions side scan can produce higher resolution images than either aerial or satellite, while still maintaining a much wider coverage in shallow environments when compared to multibeam echosounders.

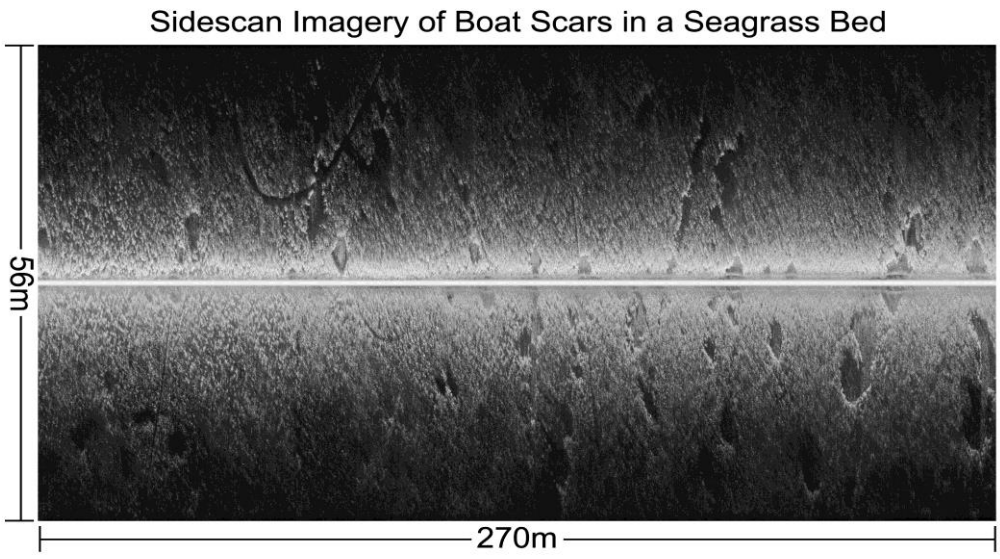

Figure 2, SSS imagery taken at 800 kHz in a disturbed bed of *Thalassia testudinum*. Areas of high reflectance (seagrass) are represented as being brighter than areas of low reflectance (bare patches). Intensity and reflectance decrease as distance from transducer increases. The bright horizontal line in the image center represents water column reflectance directly under the vessel's center where acoustic intensity is greatest – this region is removed via slant-range processing.

Methods

Collection of Satellite Imagery Standard

Satellite imagery of the test site was obtained through an imagery grant by the Digital Globe Foundation. The imagery granted was collected on 05 April 2016 via WorldView3 satellite and featured a resolution of 30 cm/px, 0% area cloud cover, 10.37 area max off-nadir angle, 64.72 minimum sun elevation, and low turbidity or reflectance over the study site (DigitalGlobe Catalog ID#056056826010, Digital Globe Inc Westminster, CO). The panchromatic band of the satellite image was used to generate a statistic for the error of corrected drone imagery and to ensure drone surveys represented accurate real-world estimates of bare

patch area. Satellite data was also used as a standard against which to compare SSS measurements for patch area.

Collection & Validation of Aerial (Drone) Imagery Standard

Aerial photography from a DJI Phantom 3 Professional drone (Dà-Jiāng Innovations Science and Technology Co., Shenzen, China) was collected on 23 August 2016 at an altitude of 100m to be used in addition to satellite imagery as a high-resolution "real world" representation of habitat structure (seagrass, bare patches, boat scars, etc) within the test plot (Fig. 3). When considering side scan representations of habitat structure, these aerial images were used as a control and treated as a standard of aerial photographic methods against which to measure sonar error. Effective pixel size at the survey altitude of 100m was calculated from formulas for vertical field of view, horizontal field of view, swath dimension, and known specifications of the drone's manufacturer supplied camera (35mm equivalent sensor dimensions as 36mm x 24mm & 35mm equivalent focal length as 20mm, sensor aspect of 3:2).

1. $\text{Vertical Field of View} = 2\ \text{atan}(\frac{0.5 \times \text{Sensor Height}}{\text{Focal Length}})$
2. $\text{Horizontal Field of View} = 2\ \text{atan}(\frac{0.5 \times \text{Sensor Width}}{\text{Focal Length}})$
3. $\text{Survey Image Swath Dimension } (X \text{ or } Y) = (X \text{ or } Y \text{ Field of View}) \times \text{Altitude}$
4. $\text{Pixel } Y \text{ Dimension} = \frac{\text{Along-Track Swath}}{\text{Image Height in Pixels}}$
5. $\text{Pixel } X \text{ Dimension} = \frac{\text{Across-Track Swath}}{\text{Image Width in Pixels}}$

The calculated values for *X* and *Y* pixel dimension (corresponding to across-track and along-track pixel size) were applied to aerial survey images in ERDAS Imagine and used to re-project drone imagery using a WGS1984 UTM Zone 14N projection based on the latitude and longitude

recorded by the drone at time of image capture. These calculations ensured all drone images utilized a uniform pixel size. Drone correction was validated by comparing the areas of bare patches observed in both drone and satellite images and calculating residual mean square error. SSS imagery was later compared to both the satellite and drone aerial standards. The area of target features was calculated in ArcMap 10.3 using the freeform feature creation tool and measured in m^2. Sixty-eight bare patches with clearly defined edges were used for validation of SSS imagery to the drone standard. Thirty-two of these features were not visible in satellite imagery due to lower resolution (0.30 m/px) or increased algal cover at time of capture (satellite: 05 April 2016 vs drone/sonar: 23 August 2016), reducing total features to 36 when comparing the satellite standard to either drone or SSS imagery.

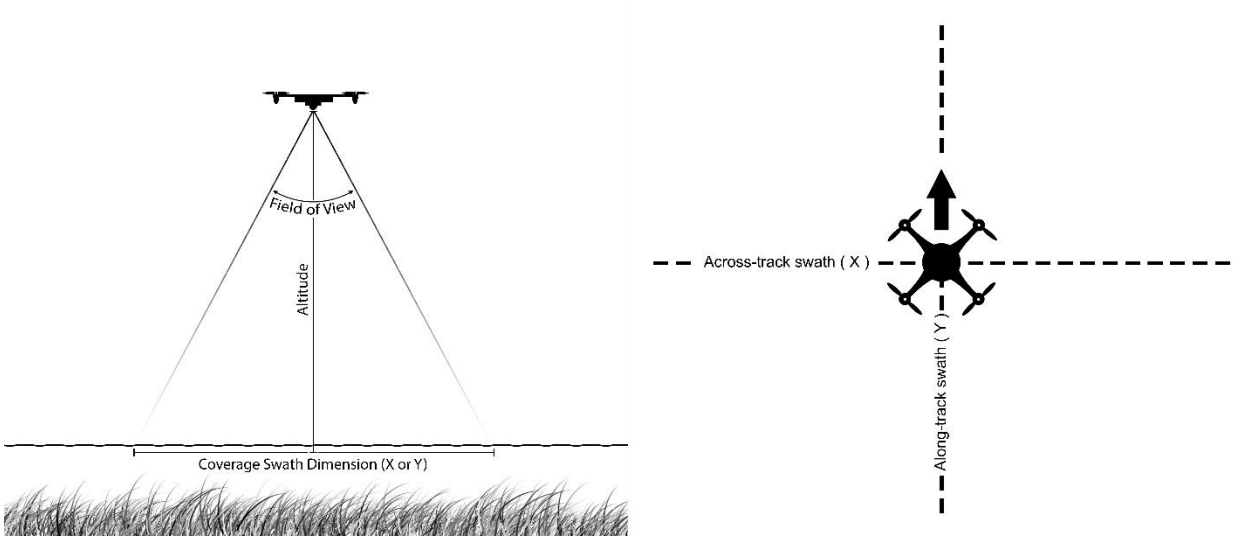

Figure 3, an example of the factors contributing to a calculation of image coverage swath in the *X* (across-track) or *Y* (along-track) dimension given known altitude and field of view.

Construction of Side Scan Echosounder

SSS used to study the sea bottom can be prohibitively expensive, often ranging into the tens of thousands of dollars (Appendix 1). The cost of SSS units can inhibit research in areas

where such resources are not available. All SSS units work fundamentally in the same way with most increases in cost due to features not typically utilized when operating in very shallow conditions (pressure sensors, etc.). We set out to produce an economical (< $2,000 USD) and robust tool which would function well in shallow coastal waters typical of seagrass habitats. To achieve this the following components were combined from readily available recreational fishing echosounders:

- 2 Lowrance StructureScan HD LSS-2 465/800 kHz side scan transducers ($180 ea.)
- 1 Dual Beam 200 kHz bathymetric sounder ($115 ea.)
- 1 Humminbird 998C HD SI echosounder head unit/controller ($1,265 ea.)

We chose to use the LSS-2 465/800 Lowrance transducers for their length when compared to other side scan transducers. Array length is a limiting factor in all side scan configurations, with longer arrays capable of producing higher resolution images for a given frequency (Key, 2000) The Humminbird HD SI control unit was selected for its ease of use and file-format compatibility with a wide range of third-party processing software. The 200 kHz bathymetric sounder was selected as it is widely available and functions well in shallow environments.

The side scan transducers used are capable of scanning at either 465 kHz or 800 kHz. Both side scan transducers were mounted on an angled acrylic plate which allowed a shallow transducer angle of 25º for increased horizontal illumination over a shallow seagrass canopy (Fig. 4). Through error and trial, we determined that a 25º transducer angle produced good results in depths ranging from 0.5 – 20 m with a swath ratio of approximately 25:1 in shallow conditions. Transects conducted over seagrass in 1 m of water would feature a total swath width of 50 m. Total cost after manufacturing of a 25 º beam angle plate was approximately $1,740 before mounting components to a static “towfish” for mounting to a vessel bow.

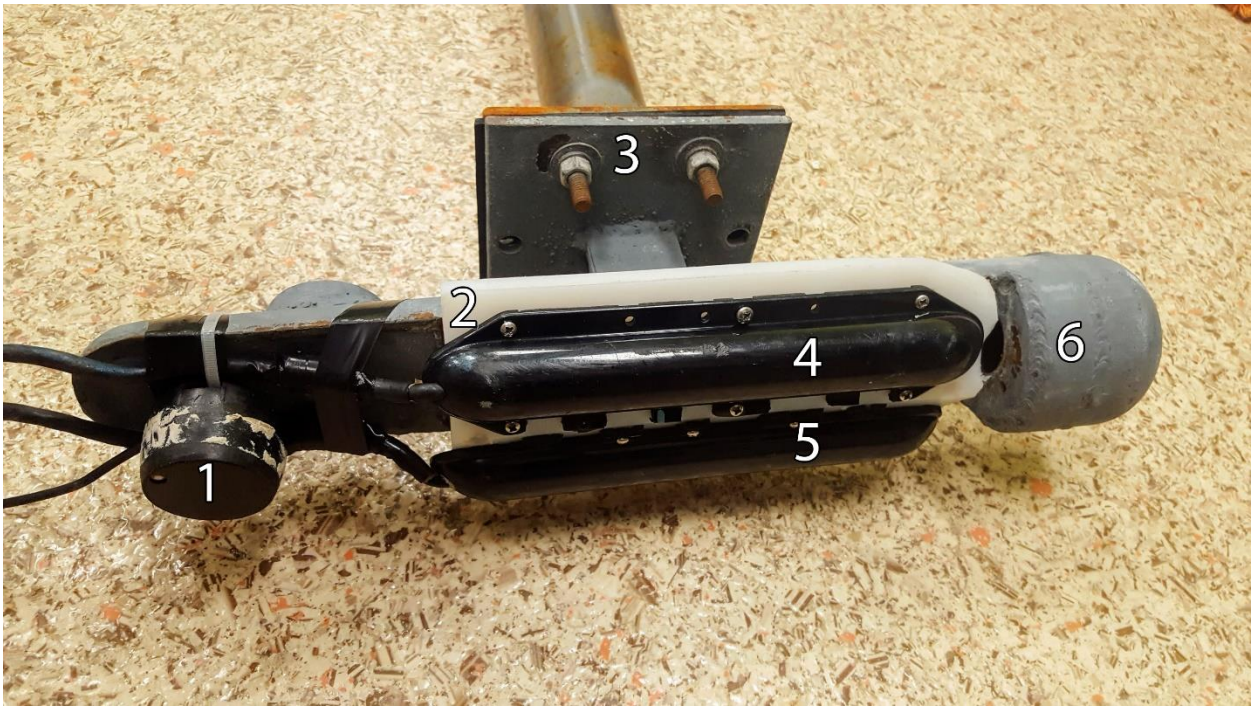

Figure 4, components of bow-mounted side scan array: 1 – bathymetric sounder, 2 - angled plastic transducer mounting plate, 3 - attachment point to vertical bow-mount, 4 - starboard side scan transducer, 5 - port side scan transducer, 6 - streamlined head to smooth water flow over transducers.

Collection of Sonar Data

Our apparatus was arranged as a static, bow-mounted design to avoid propeller wash in shallow conditions. The transducer array was mounted onto a vertical pole off the vessel's bow 30 cm below the surface with a fixed orientation in line with vessel direction of travel. This static mount also reduced yaw effects typically associated with towed arrays. A GPS receiver was mounted above and approximately 12 cm behind the center of the transducer staves on a horizontal plate, and communication was established by running cables from both the fixed sonar array and the GPS antenna to the echosounder head unit. Recordings were made at a frequency of 800 KHz in straight-line transects at a speed of 1.5 m/s in a variety of weather and water

conditions. Sonar readings were only affected in especially high wind-chop and this problem was avoided entirely if traveling in a leeward direction. Sites requiring multiple transects were scanned with approximately a 50% overlap between swaths. Transect lines were planned in the free ship navigation software OpenCPN. To maintain minimal cost, no motion control unit was used to correct for ship motion (roll, pitch, yaw, heave, etc) and all errors associated with these vessel motions would be assumed as originating from the side scan array. Use of a motion control unit would likely improve results under decreased survey platform stability albeit at a significantly increased cost.

Two types of SSS transects were collected at two sites to meet data requirements. Six parallel 600 m long transects were collected along the middle of the test plot with approximately 50% overlap. These transects covered a total area of approximately 88,000 m^2 and served as a test of the ability of side scan to function in a shallow, heterogeneous seagrass bed. A secondary set of side scan transects was also collected at a separate site of similar depth without seagrass and minimal algal cover. Both survey sites had an average depth of approximately 0.8 m. Prior to data collection at the bare site, an array of six large tires of known dimensions was submerged and anchored in place to serve as standardized targets. Comparisons between the known dimensions of these tires and their SSS recorded dimensions were used to generate insights into the distortion and error present when operating side scan in very shallow conditions (< 3 m). A basic slant-range correction was applied to all SSS files (SonarTRX). This ensures researchers can expect to replicate this study's findings with minimal post-processing of SSS data.

Describing Side Scan Sonar Distortion

Mazel (1985) and Lurton (2002) described the relationships of beam width, beam thickness, and how these factors may alter a target's representation in side scan imagery. Pulse

thickness is a direct product of both sound velocity in the water column, and the length of the pulse. Pulse thickness is directly related to the across-track resolution of the wave as it travels horizontally away from the transducer. Close to the transducer beam footprint and pixel size are large, which may horizontally stretch a single target, or stretch two nearby targets to appear as a single target (Fig. 5). As distance increases, the across-track footprint of a side scan wave is reduced, distortion is reduced, and horizontal resolution is increased.

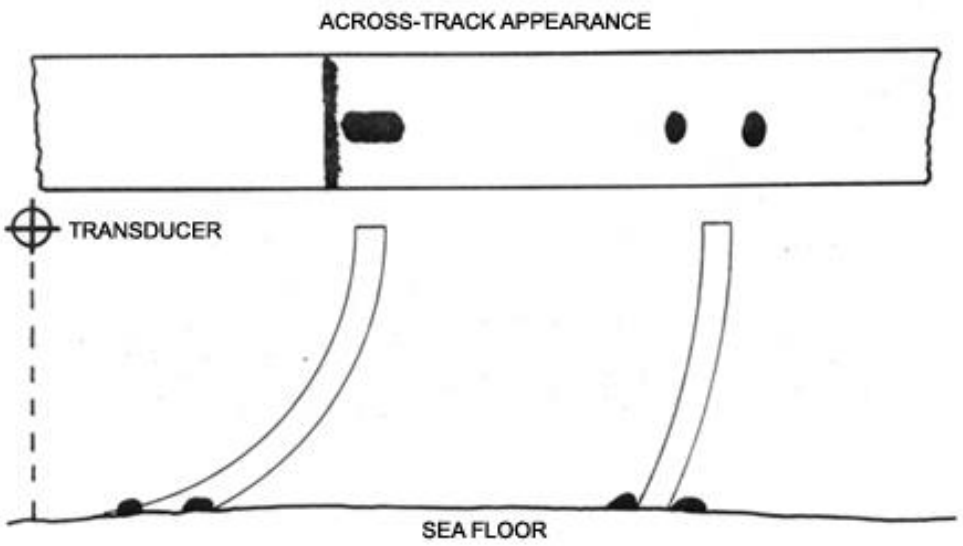

Figure 5, representation of across-track target appearance at near and far distances from a transducer (adapted from Mazel, 1985 and Lurton, 2002).

Along-track distortions, those that happen in the direction of vessel travel, are directly related to the horizontal beam-width of the survey. Targets close to the transducer, where beam width is narrowest, will experience reduced along-track distortion. As distance from the transducer increases, beam width will increase. This will result in increased along-track pixel size, reduced resolution, and increased along-track distortion. A target at great distance may appear stretched along the direction of transducer travel, and two nearby targets may appear joined as one (Fig. 6). The result of across-track and along-track distortions can cause significant

changes in how a target is represented in side scan imagery. At a given distance from the transducer a target may appear wider or taller than it is. Additionally, at some distance from the transducer across and along-track distortions should cancel out, producing a target image with an aspect equal to that of the real target. These interactions have been poorly studied in the unique acoustic environment of a shallow seagrass bed. We aimed to quantify the effect of these distortions on a survey of features (bare patches in seagrass meadows) using consumer-grade side scan.

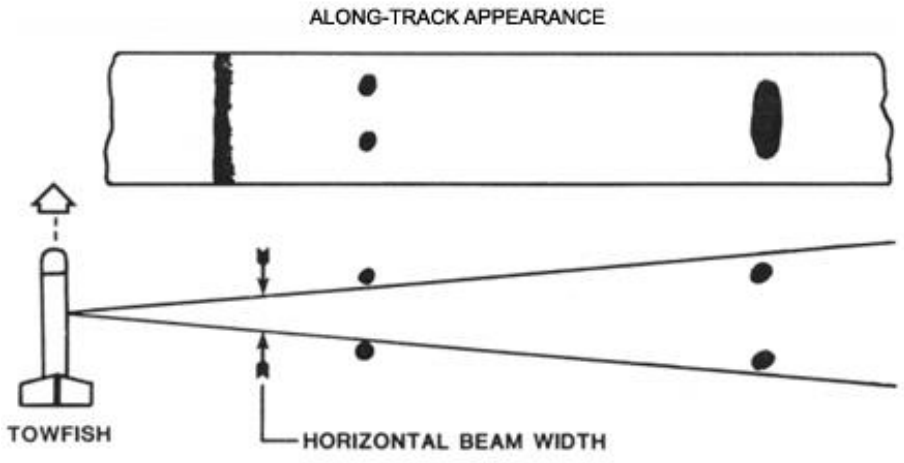

Figure 6, representation of along-track target appearance at near and far distances from a transducer (adapted from Mazel, 1985 and Lurton, 2002).

Quantifying *in-situ* Side Scan Distortion Using Known Submerged Objects

To quantify along-track and across-track distortions of our side scan array we deployed an array of six large tires. Tires were deployed and anchored in a straight line at a depth of 0.8 m in a flat area devoid of any seagrass and with minimal algal cover (Fig. 7). Straight-line distance between tires was measured *in-situ*. Tire diameter was measured prior to deployment. For all

comparisons side scan transects were collected at varying distances from the tire array at perpendicular, parallel, and oblique angles to represent a wide variety of survey paths relative to target position. Scans were performed at a frequency of 800 kHz, the same frequency used in scans of the large seagrass test plot. Sonar data was slant-range corrected in SonarTRX to best represent the simplest corrected SSS data most researchers would have access to. The following comparisons were made:

- Actual vs sonar-recorded tire diameter in the along-track direction as a function of distance from transducer
- Actual vs sonar-recorded tire diameter in the across-track direction as a function of distance from transducer
- Actual vs sonar-recorded tire aspect (across track diameter / along track diameter) as a function of distance from transducer

Respectively, these three comparisons would provide functions for along-track distortion, across-track distortion, and distortion of shape. While not in the scope of this study, the inverses of these functions could potentially be used to mathematically correct similar SSS data and further reduce error.

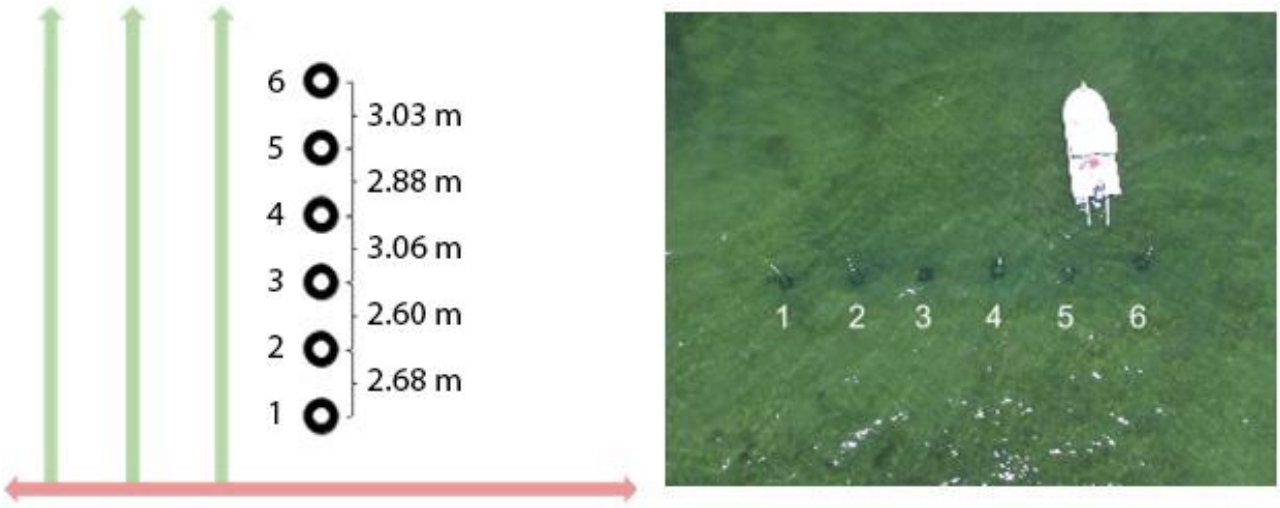

Figure 7, a demonstration of the deployed tire array and example boat paths while collecting side scan of the target tires. Transects varied by angle and distance to target array. Tire diameters were measured as: Tire 1: 73.0 cm, Tire 2: 69.0 cm, Tire 3: 73.8 cm, Tire 4: 73.5 cm, Tire 5: 69.5 cm, and Tire 6: 73.8 cm.

Data Handling

All sonar data used in this study consisted of image files generated onboard the Humminbird 998C SI HD head unit. Side scan imagery was then processed for slant-range correction in SonarTRX and subsequently exported as a GeoTiff (.tif) file format (Ritter & Ruth, 2000). GeoTiff SSS files complete with track location data were imported into ArcMap 10.3 and projected using WGS1984 UTM Zone 14N. From recorded track points a single continuous center-track line was generated for all measured transects using the "Points to Line" tool in ArcMap. All area measurements taken from drone, SSS, and satellite imagery were done using either the freeform or ellipse polygon feature class creation tool in ArcMap by drawing the outline of the target feature at high magnification as closely as image resolution allowed. Polygons created from drawn features automatically have their area in m^2 calculated in ArcMap. In all cases features without clear borders from bare sediment to the surrounding seagrass meadow were avoided. Distance measurements, such as those from transducer (center-track line)

to target, were calculated using the ruler tool in ArcMap to calculate the perpendicular path distance from target to transect center line. For visualization purposes only (Appendix 2) a mosaic of all SSS transects was automatically generated in SonarWiz using automatic gain correction and beam-angle processing not included in the rest of this study.

Sonar Operating Parameters

Data collection on the Humminbird 998C HD SI head unit controller was performed at the following internal settings and recordings made using the default recording interface:

- Beam select (Bathymetry): 200/83 kHz
- SI Imaging Frequency: 800 kHz
- Surface Clutter: 5
- Fish ID +: Off
- Fish ID Sensitivity: 5
- RTS Window: Narrow
- SI Sensitivity: 3
- Max SI Range: 100 ft
- Chart Speed: 5
- SI Side: Both

Results

Sonar Calibration

Twelve SSS transects taken over an array of six submerged tires were used to generate distortion data for along-track and across-track directions. Eighty total measurements were taken comparing actual target diameter to sonar-recorded along-track or across-track diameter.

Residuals of sonar-derived and actual diameters (sonar-derived – actual) were plotted as a function of distance from transducer to target. A preliminary assessment grouped root mean squared error (RMSE) of these measurements every 3 m to better highlight regions of increased distortion within the horizontal range. This assessment showed unusually high across-track distortion at distances less than 3 m (Fig. 8, Fig. 9). Curves were generated for data both with and without these samples in Fig. 10 and Fig. 11 to demonstrate reduced error after removing the first 3 m of uncorrected SSS data. Across-track and along-track distortions were plotted separately to better highlight how each influence uncorrected SSS imagery. Many factors affect sonar distortion such as vessel movement (heave, sway, roll, etc.), vessel speed, water depth, and distance to target. Given this complex relationship and limited *in-situ* testing a second-degree polynomial fit was chosen over a linear fit. Aspect residuals (sonar across-track diameter / sonar along-track diameter) were plotted as a function of distance from transducer to demonstrate the interactions of both distortions on an observed target at varying distances from a survey vehicle. Linear fit lines were included to demonstrate a simplified model of across-track or along-track distortion effects (RMSE) across the distance groupings.

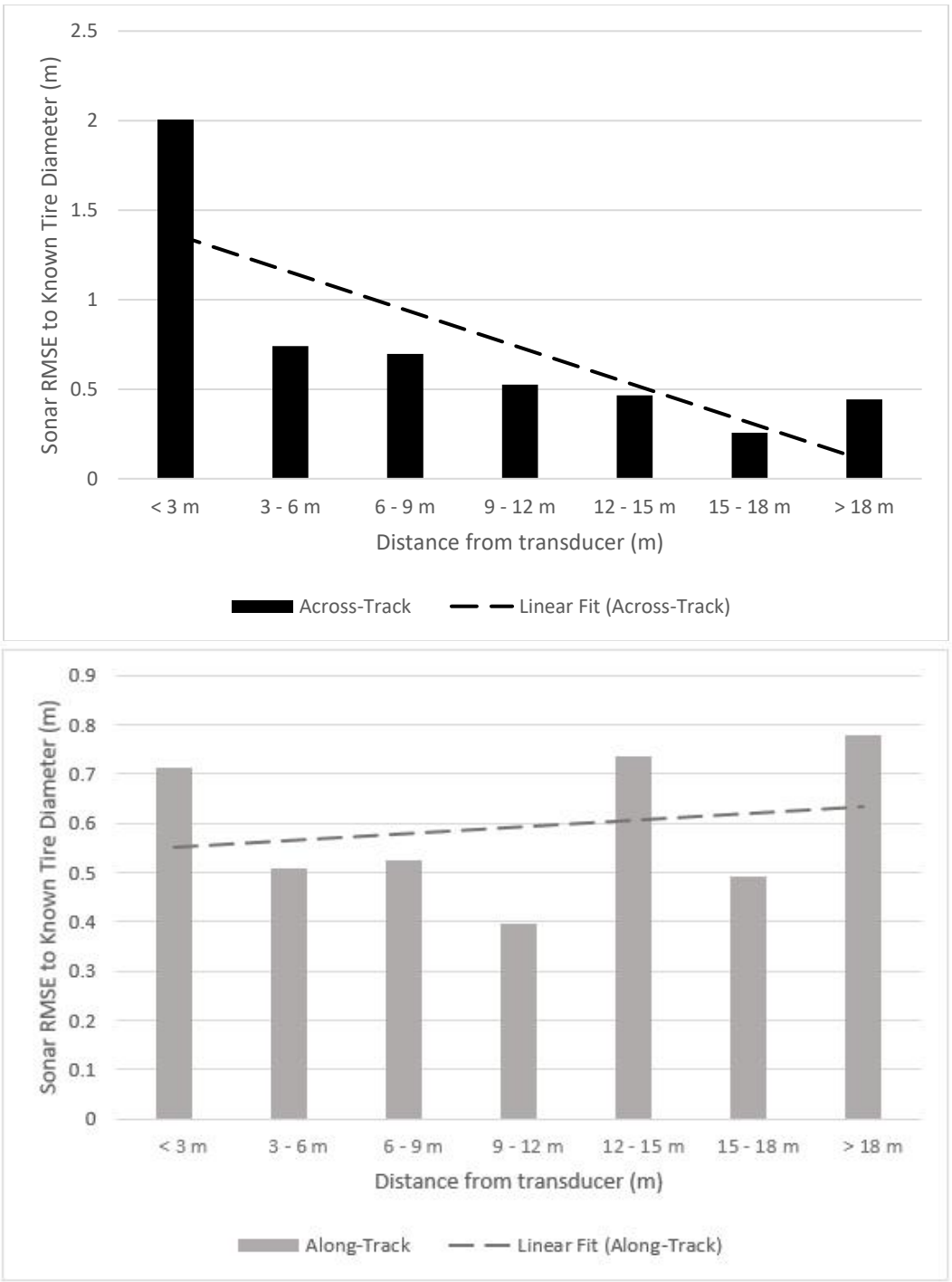

Figure 8, RMSE of sonar measurements compared to actual tire diameter in the across-track (top plot) and along-track (bottom plot) direction. In both plots RMSE is grouped by distance from transducer.

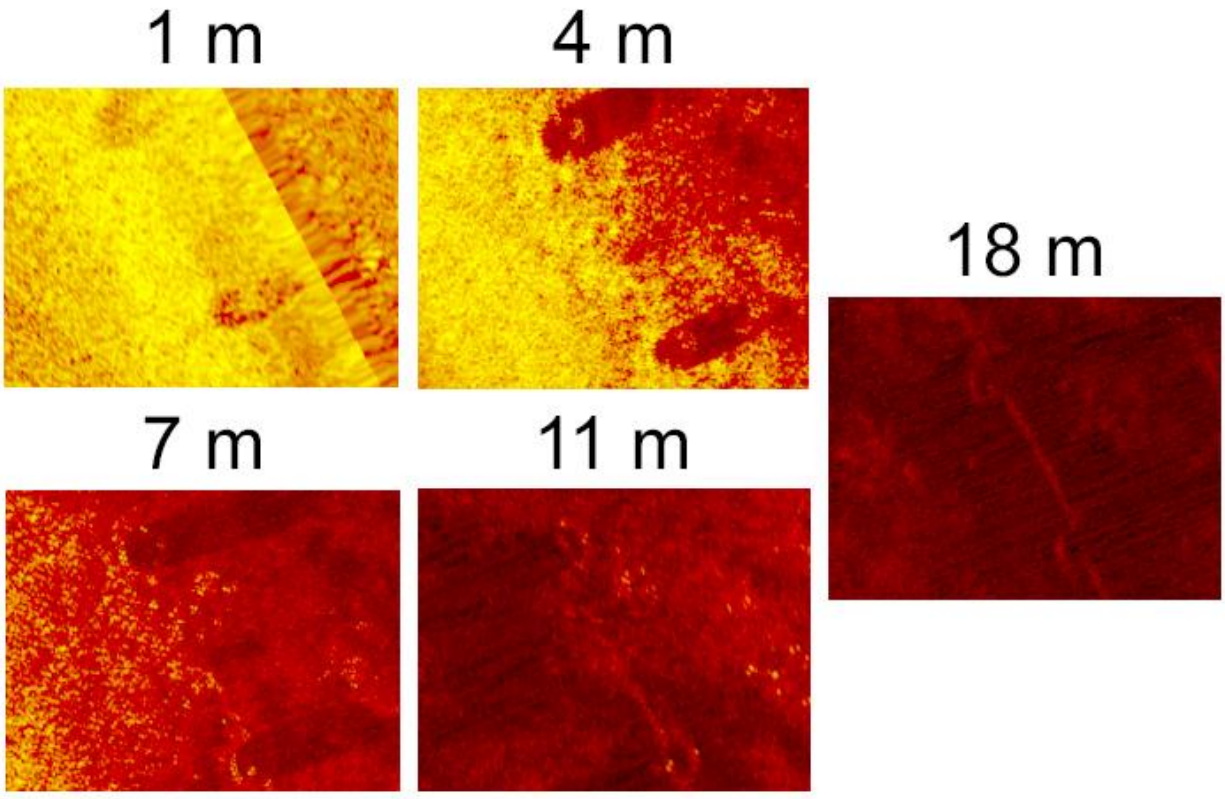

Figure 9, screen captures taken during sonar testing of target tires at 1 m, 4 m, 7 m, 11 m, and 18 m distance intervals from the transducer. Targets at 1 m appear heavily distorted, and target visibility is reduced as distance from transducer increases.

Calculations indicate along-track distortion (stretching of target in the direction of vessel travel) increases throughout side scan horizontal range. These results fit the theoretical model provided by Mazel (1985) on how a side scan wave should render targets at increasing distances where along-track distortions increase with increasing distance from target to transducer (d). Residuals between known tire diameter and along-track diameter ($R_{along\text{-}track}$) averaged 0.077 m (standard deviation (σ) = .143 m) with an RMSE of 1.43 m (Fig. 10). The formula of a second-degree polynomial fitted to along-track distortion data as a function of distance from transducer was:

6. For all samples: $R_{along\text{-}track} = -0.00005d^2 + 0.0033d + 0.054$
7. Excluding samples closer than 3 m: $R_{along\text{-}track} = -0.0001d^2 + 0.005d + 0.047$

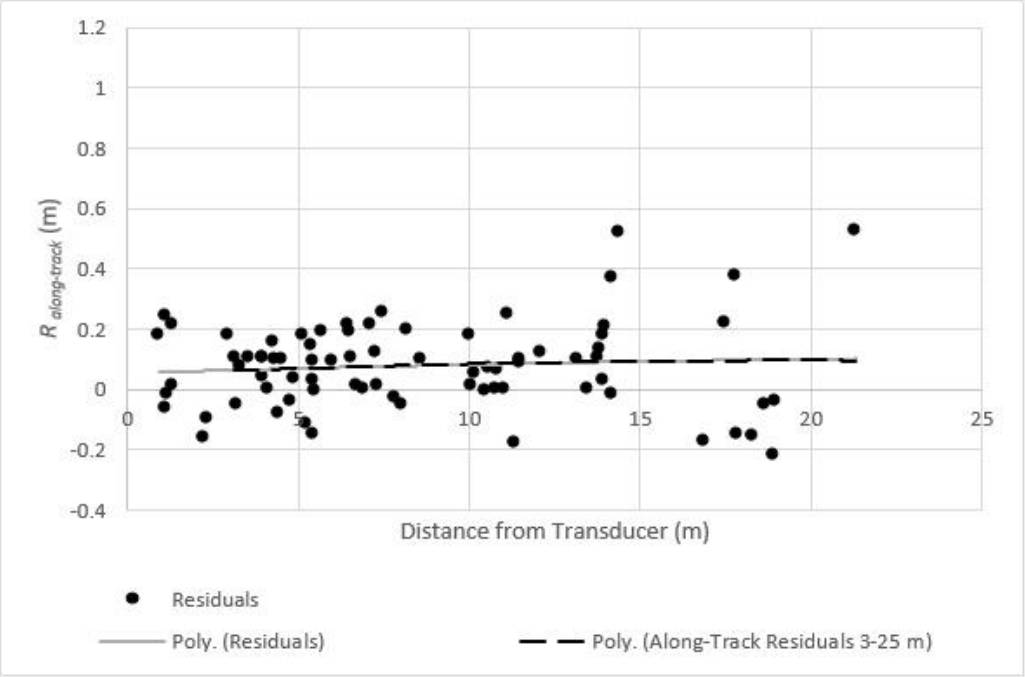

Figure 10, residuals in the along-track direction (along-track diameter – actual diameter) as a function of target distance from transducer. A Y-value of 0 represents 0 m of distortion in the along-track direction.

Measurements for across-track distortions also hold to theoretical expectations. Across-track distortion (stretching of a target perpendicular to direction of vessel travel) was maximized at both short (< 3 m) and long horizontal ranges (> 19 m) (Fig. 11). Mid-range distances of 10 – 15 m from transducer showed the least distortion. Across-track results also closely fit the theoretical model laid out by Mazel (1985) where across-track distortion is greatest close to the transducer, and decreased with distance (*d*). Residuals from across-track distortion ($R_{across\text{-}track}$, across-track target diameter – known target diameter) averaged 0.18 m (σ = 0.21 m) with an RMSE of 2.41 m. When samples from the first 3 m of horizontal range were removed, average distortion reduced to 0.12 m (σ = 0.11 m), RMSE was reduced to 1.34 m, and the fit line more closely matched Mazel's model (1985). The formula of a second-degree polynomial fitted to across-track distortion data as a function of distance from transducer was:

8. For all samples: $R_{across\text{-}track} = 0.0033d^2 - 0.0857d + 0.5762$

9. Excluding samples closer than 3 m: $R_{across\text{-}track} = 0.0003d^2 - 0.11d + 0.1899$

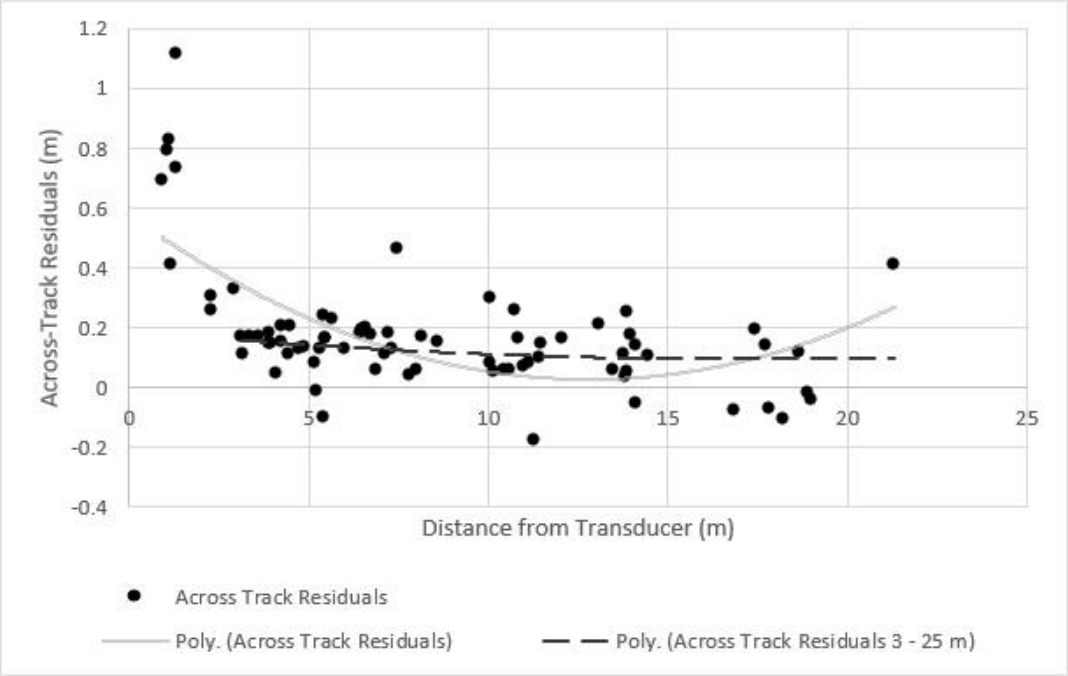

Figure 11, residuals in the across-track direction (across-track diameter – known diameter) as a function of target distance from transducer. A Y-value of 0 represents 0 m of distortion in the across-track direction

The relative contributions of the above across and along-track distortions on a target's shape can be visualized by plotting the aspect (across-track diameter / along-track diameter) of sonar-recorded targets at varying distances (Fig. 12). These round targets would feature an aspect of 1 under zero distortion. Measurements indicate that targets closer than 9 m and farther than 16 m will appear increasingly stretched horizontally (across-track). Targets at intermediate distances of 9 – 16 m from the transducer will appear stretched vertically as along-track distortions are maintained but across-track distortions are minimized in this zone. After removal of the first 3 m of horizontal range, the relationship of across-track to along-track distortion (aspect) becomes

nearly constant. These results indicate that removing the first 3 m of data could greatly simplify secondary image correction and target measurement.

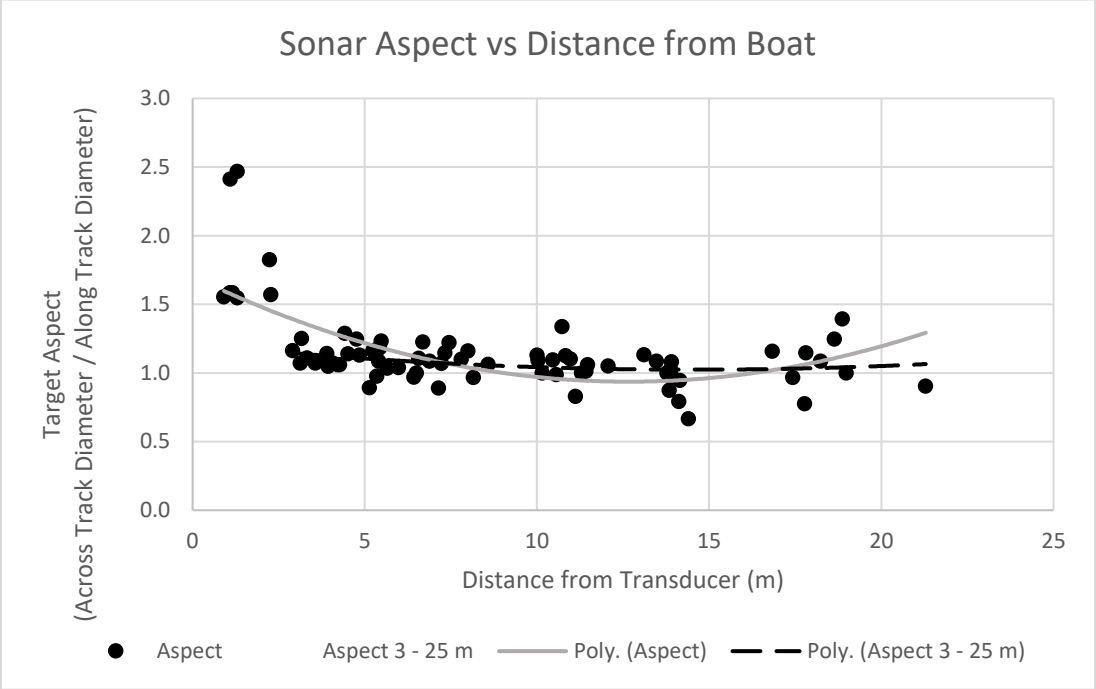

Figure 12, aspect (across-track diameter / along-track diameter) for 80 tires measured at varied distances from the side scan transducer. Y values of 1 indicate a round tire with no distortion of shape. Positive values indicate dominant across-track stretching, and negative values indicate dominant along-track stretching.

Validation of Aerial Drone Standard to Satellite Standard

Calculations for effective pixel size in drone survey imagery taken from 100m altitude yielded a horizontal field of view of 84° and a vertical field of view of 61.9°. These calculations were based on a 35mm equivalent for the drone's camera sensor of 36mm x 24mm (3:2 aspect ratio), and a 20mm equivalent focal length. From the survey altitude, an image footprint was calculated to be 180m wide and 120m tall on the ground. Dividing footprint values by image dimensions of 3992 x 2992 pixels, effective pixel size was calculated to be 4.51 cm/px wide by 4.01 cm/px tall. To validate the adjusted drone imagery, 36 bare patches from within the seagrass

test site were measured for area both in the satellite standard and in the corrected drone imagery. Measurements showed high agreement with corrected drone imagery over-estimating bare patch area by 3.75% on average ($\sigma = 0.18$, RMSE = 15.62 m^2) (Fig. 13). These results were satisfactory to use the corrected drone imagery as a suitable standard for aerial imagery against which to compare sonar measurements.

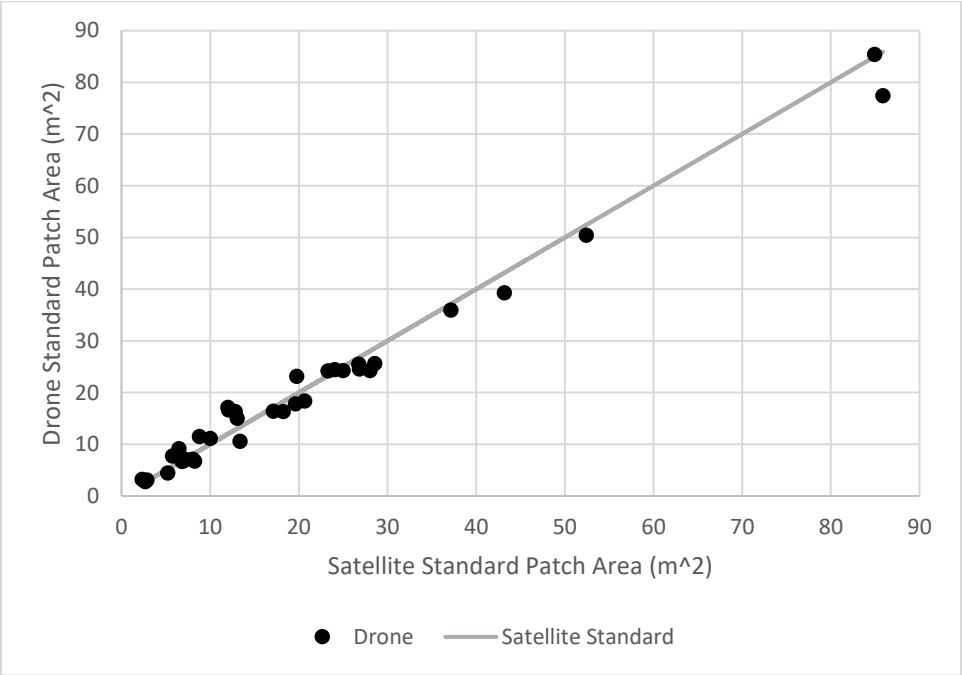

Figure 13, drone-calculated versus satellite-calculated area measurements for 36 bare patches selected from within the test site. Points indicate drone-calculated bare patch area relative to satellite-calculated area for the same feature. A line is included for comparison and represents the condition of drone and satellite measurements being in complete agreement.

Validation of Side Scan to Satellite Standard

The same 36 features used to validate drone imagery were also used to validate SSS imagery to the satellite standard. Measurements taken from SSS over-estimated bare patch area by an average of 20.27% ($\sigma = 0.28$) with an RMSE of 22.18 m^2 when compared to the satellite standard (Fig. 14).

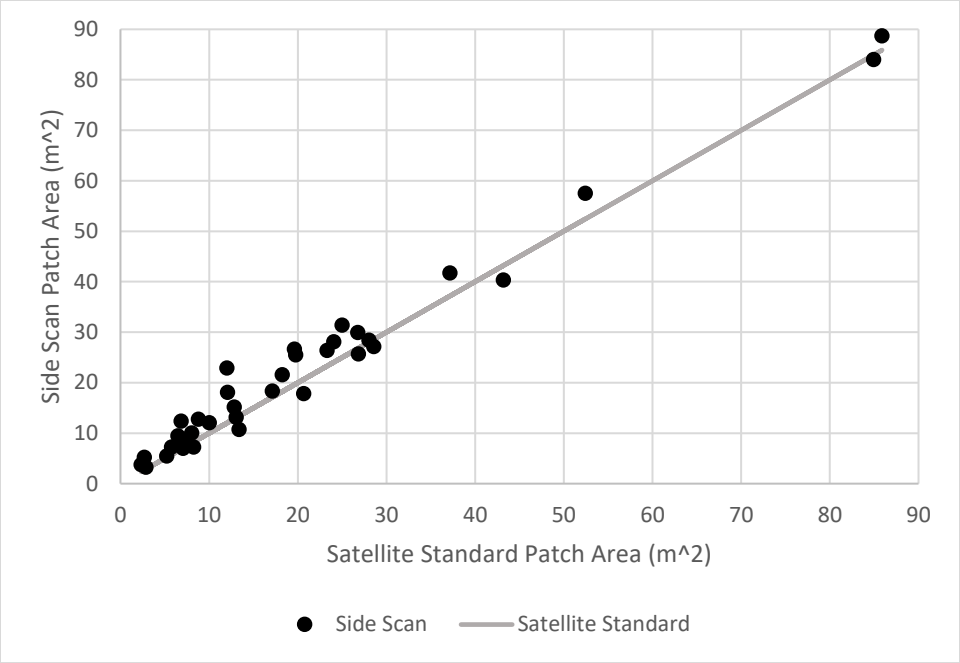

Figure 14, sonar-calculated versus satellite-calculated area measurements for 36 bare patches selected from within the test site. Points indicate sonar-calculated bare patch area relative to satellite-calculated area for the same feature. A line is included for comparison and represents the condition of sonar and satellite measurements being in complete agreement.

Validation of Side Scan to Aerial Drone Standard

In addition to the 36 features used in comparisons with satellite imagery, increased resolution of drone imagery and capture immediately before conducting sonar operations increased comparable patches between drone and SSS imagery to a total of 68. The area of these 68 patches were measured between uncorrected SSS imagery and the drone standard in the same manner as previous comparisons (ArcMap 10.3, freeform feature creation tool). It was found that side scan imagery over-estimated patch area by an average of 13.15% ($\sigma = 0.22$, RMSE = 28.33 m^2) (Fig. 15). Over-estimation was most prevalent in features which occurred on the edges of the side scan horizontal range, fell along the center line, or were scanned during a period of change in the vessel's course. Examples of high and low-agreement between side scan and aerial imagery are provided in Figure 16. Error is very likely the result of acoustic distortions (along

and across-track) acting on measured features, and highlights potential improvement by fully correcting these distortions in post-processing. Incorporating overlap between scan transects also affords freedom to select those targets which fall into the horizontal range of multiple recordings and allowing error to be reduced with subsequent measurement.

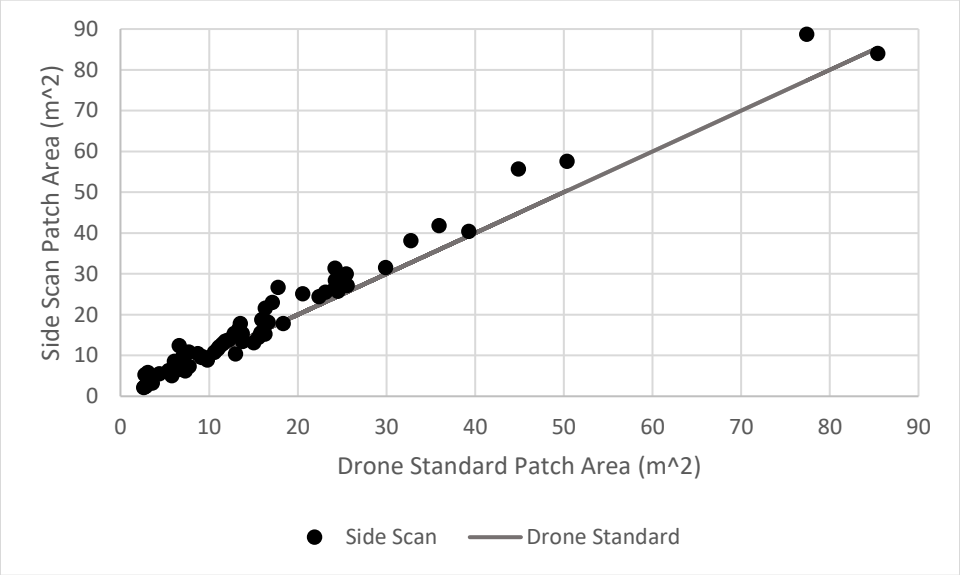

Figure 15, sonar-calculated versus drone-calculated area measurements for 68 bare patches selected from within the test site. Points indicate sonar-calculated bare patch area relative to drone-calculated area for the same feature. A line is included for comparison and represents the condition of sonar and drone measurements being in complete agreement.

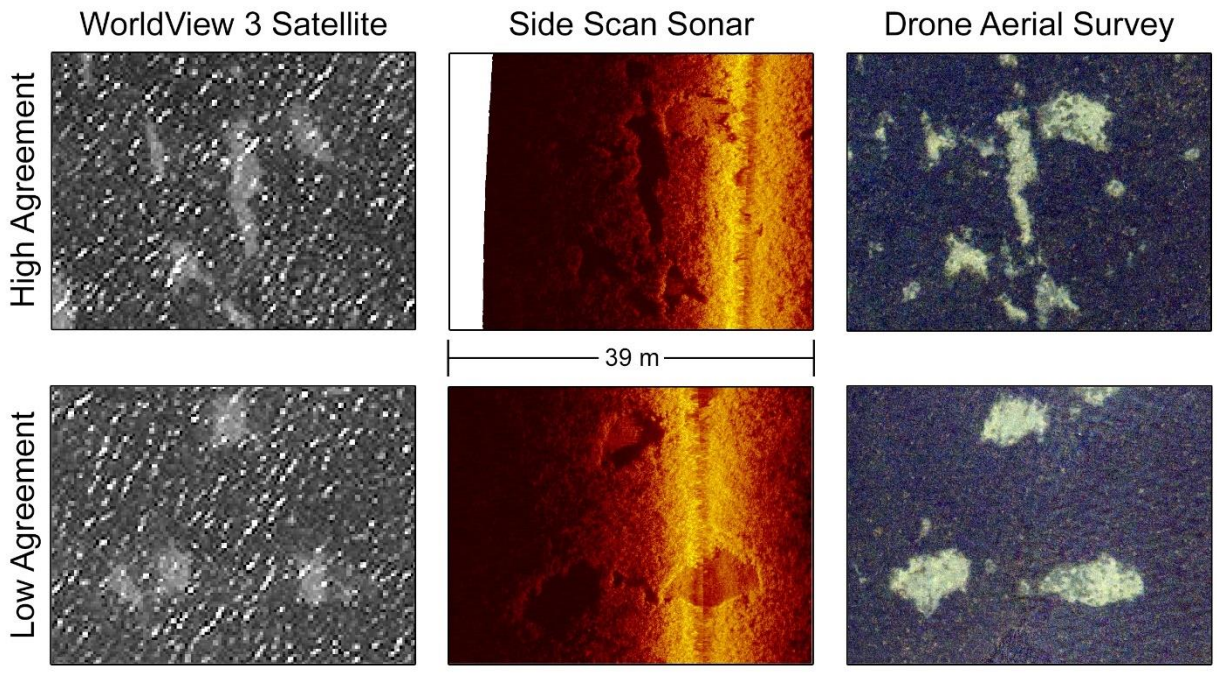

Figure 16, examples of high and low-agreement between satellite (WorldView 3), side scan sonar, and drone aerial surveys. Features which fall under the center line of a transect are likely to be distorted during the slant-range correction process.

Discussion

Use of Side Scan in Shallow Seagrass Meadows

The results of this chapter demonstrate that an inexpensive side scan array (Appendix 1), developed from consumer-grade components, can produce high-resolution imagery of a shallow seagrass bed (< 2 m). Seagrass ecosystems in this depth range are widely underrepresented in the literature of acoustic seagrass surveys and often cited as too shallow to efficiently study with acoustic instruments (Sagawa et al., 2008 ; Sabol et al., 2002 ; Paul et al., 2011 ; Lefebvre et al., 2009 ; DeFalco et al., 2010). These results are in direct contrast to previous works which claim acoustic instruments such as SSS cannot produce data of adequate quality in shallow conditions.

The array described is demonstrated to over-estimate the area of features by approximately 13.15% with minimal corrections applied (slant-range only) when compared to aerial surveys. Accuracy may be further improved by mathematically correcting along-track and across-track distortions, or by removing the first 3 m of horizontal range where distortions are most dramatic. Acoustic studies of seagrass meadows at depths of 1 – 3 m are poorly represented in the literature despite shallow meadows suffering increased risk of fragmentation. This work represents a valuable *in-situ* study of SSS functionality and distortion characteristics when used in very shallow conditions with both known target objects and natural features. The described array provides a new tool for measuring shallow seagrass habitats not well represented in the literature of acoustic surveys or for surveying macrophyte beds under conditions which limit aerial or satellite techniques. Features such as boat scars, bare patches of varying sizes, and algae-filled bare patches are all clearly imaged without additional post-processing – and results may be further improved with the use of software to correct beam angle and signal gain (Appendix 2). With a low cost compared to commercial side scan units, the array demonstrated in this work provides an inexpensive and flexible instrument for resource-limited researchers who cannot access commercial echosounders.

Error from Drift Algae in Satellite and Aerial Imagery vs Side Scan

It was observed in this study that bare patches in seagrass meadows may seasonally fill with a thick matte of drift algae. This action can significantly reduce the visibility of affected bare patches in both satellite and aerial imagery, and may lead to significant over-estimations of seagrass coverage without special attention. Of the 68 bare patches measured in our aerial standard captured 23 August 2016, only 36 of these features were visible in the satellite standard (resolution: 0.30 m/px) captured 05 April 2016. All missing features were present prior to the

satellite capture date, indicating their cryptic nature once filled with drift algae. Difficulty in discerning these algae-filled features persists even with the low altitude and high resolution of drone aerial imagery, and drastic differences in perceived total bare area can be observed when comparing drone surveys before and after drift algae influx. Due to the acoustic properties of algae being different from the surrounding seagrass, algae-filled bare patches can be clearly seen in all side scan imagery as if no algae were present (Fig. 17). These findings suggest a strong utility for side scan surveys in areas where algae cover is high, or as a tool for validating the results of optical surveys under these conditions.

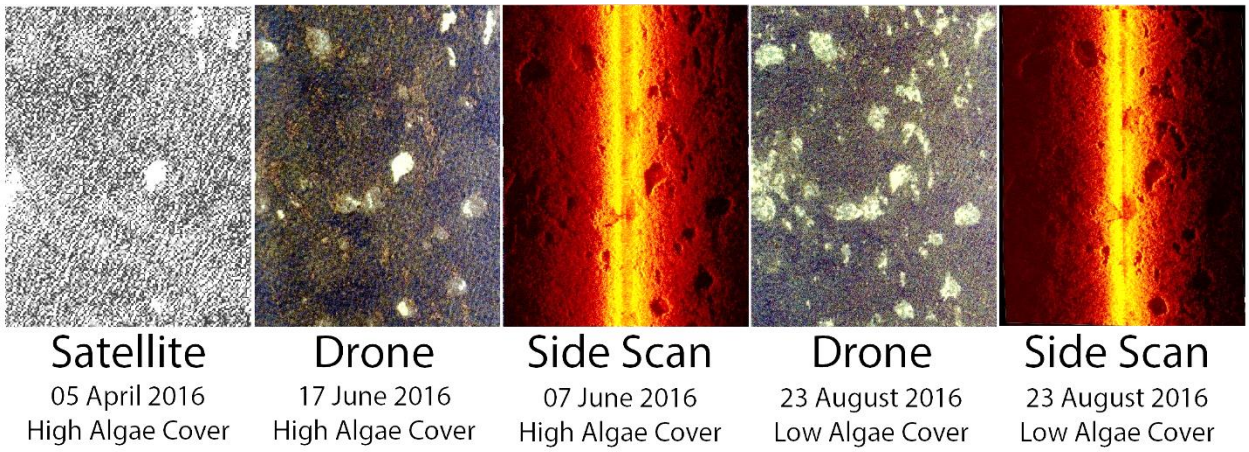

Figure 17, same area within the test site taken from 05 April 2016 to 23 August 2016 demonstrating multiple levels of algal cover and its influence on satellite imagery, high-resolution aerial imagery, and side scan imagery.

Potential Issues with Side Scan Surveys in Shallow Seagrass Beds

Side scan arrays constructed from inexpensive materials such as those used in this study may represent a unique, cost-effective tool for many researchers working in shallow bays – but these methods are not without their own complications. Correction of side scan imagery becomes increasingly complex beyond the basic utilities for slant range correction and bottom tracking offered by most sonar processing software packages. While capable of producing very high

resolution imagery, side scan is logistically limited to relatively slow survey speeds (1 – 5 m/s). Side scan also requires a steady survey platform as unexpected movements (vessel course change, sudden heave, etc) can produce large errors or distortions in imagery. Vessels chosen as survey platforms must balance minimal draft to operate in shallow conditions with optimal stability. If available, correction of data with an appropriate ship motion control unit such as that used in the next chapter may provide considerable improvements on overall accuracy however motion control units for side scan arrays appear to be scarce if available at all. While the described array can produce accurate surveys for seagrass coverage, further advancements must be made before other characteristics of the seagrass habitat such as species composition can be accurately assessed. Analyses of backscatter intensity and "pattern" may help in this regard, as has been seen in studies utilizing bathymetric or multibeam sonar for seagrass classification. Considerations should also be made for changes in bathymetric slope of the study site. The study site used in this work was largely flat and uniform in depth. It is unknown at this point if seagrass is capable of growing on slopes of significant steepness to impact SSS performance, but such considerations should be made on a per-site basis.

Suggestions for Future Work

Our study demonstrates the utility of SSS in surveying habitat fragmentation in very shallow seagrass beds where other studies have indicated use of SSS is not efficient. High survey resolution (2.5 cm/px), flexibility in suboptimal conditions (high turbidity, poor weather), and the capability to "see" through drift algae grant SSS unique utilities over both aerial and satellite survey methods. Further advancements made in both improving the resolution and distortions of side scan used in shallow conditions will greatly improve this utility. Advancements in the field of automated pattern recognition have already produced preliminary results using SSS data from

this study to demonstrate the automatic detection and measurement of bare patches within a shallow seagrass meadow (Appendix 3). Further work on pattern recognition may be extended to measure direct anthropogenic disturbances such as propeller scarring. While this study emphasizes the "out of the box" capabilities of SSS to produce reasonably accurate imagery with limited post-processing, distortion correction utilizing the distortion profiles listed previously (6, 8) may significantly improve utility by reducing error – especially in regions closer than 3 m from the transducer. Advancements in GPS receiver technologies and a cost reduction of these systems will also improve spatial accuracy.

CHAPTER III

USE OF PARAMETRIC SONAR FOR HIGH-RESOLUTION MAPPING OF SEAGRASS SEDIMENTS AND ORGANIC CARBON IN A CONTINUOUS SOIL MATRIX

Abstract

Despite a global nutrient-cycling value of $1.9 Trillion, seagrass habitats world-wide are in decline (Waycott et al., 2009). Many methods exist to measure the health of seagrass habitats, including optical, acoustic, and point-based field surveys. Assays of seagrass productivity typically include metrics for gas exchange, or involve monitoring the growth of individual blades (Zieman, 1974). Measurements of organic carbon (OC) content are infrequent, despite carbon content in the rhizosphere acting as a direct indicator of macrophyte growth over time. Limited use of OC measurements in surveys of seagrass is likely the product of the logistical complexity of removing cores from subtidal environments, the destructive nature of this sampling, and the cost of processing many soil samples. We propose the use of parametric sonar for non-destructive, remote measurement of sediment layering in a seagrass meadow to be used with a limited number of soil cores for ground-truthing. Parametric sonar is demonstrated as capable of detecting seabed reflectors beneath bare patches within a seagrass meadow. Soil profile data is used to investigate the similarity of vegetated and unvegetated sediments, and these similarities are used to infer reflectors into areas of seagrass cover where they are otherwise not visible to sonar. Estimates of total organic carbon captured in sediments above acoustic reflectors are made for a large area approximating 52,000 m^2.

Introduction

In addition to acting as a food and habitat source for many aquatic species (Lee & Dunton, 1996) and limiting erosion (Bos et al., 2007), seagrass habitats are widely recognized as a significant carbon sink. Carbon stored by marine ecosystems, known contemporarily as "Blue Carbon" has become a focus of research and management efforts worldwide as increased sequestration removes carbon from the atmosphere and helps mitigate the effects of climate change (Duarte et al., 2005 ; Bouillon et al., 2008 ; Lo Iacono et al., 2008 ; Duarte et al., 2010 ; Kennedy et al., 2010 ; Donato et al., 2011 ; Mcleod et al., 2011 ; Fourqurean et al., 2012 ; Pendleton et al., 2012 ; Lavery et al., 2013 ; Howard et al., 2014 ; Pergent et al., 2014 ; Luo et al., 2016). Global estimates of sequestration by submerged aquatic vegetation (SAV) estimate contributions as high as 19.9 Pg of organic carbon per year, accounting for up to 15% of global capture by marine systems (Fourqurean et al., 2012). Total organic carbon sequestered by seagrasses could reach up to 273 kg / m^2 in some regions (Pergent et al., 2014). Despite providing $1.9 trillion in ecosystem services SAV habitats are in global decline (Waycott et al., 2009) due to anthropogenic pressure, rising sea levels, and increasing sea surface temperatures (Pergent et al., 2014). Between 340,000 and 980,000 hectares of blue carbon ecosystems are destroyed annually (Murray et al., 2011).

Sequestration of carbon by seagrass occurs at short time scales of decades (Howard et al., 2014) yet storage may persist for thousands of years in marine sediments (Duarte et al., 2005 ; Lo Iacono et al., 2008) due to anoxic conditions (Mcleod et al., 2011). Carbon is locked into the soils of seagrass habitats by either the continuous accretion of decaying organic matter into thick vertical mattes such as in beds of *Posidonia oceanica* (Lo Iacono et al., 2008), or by the direct deposition of decaying belowground biomass (roots or rhizomes) into the soil carbon pool by

those seagrasses which are not matte-forming (Fourqurean et al., 2012). Above-ground decaying biomass (dead leaves or shoots) and below-ground living biomass (living roots or rhizomes) do not represent significant stores of carbon in seagrass systems (Howard et al., 2014). The Intergovernmental Panel on Climate Change reported in 2007 that atmospheric carbon-dioxide levels must be reduced by 85% by the year 2050 to avoid a 2°C increase in global temperatures (IPCC, 2007). The study and management of carbon pools such as those in seagrass soils have been recognized as a critical tool in achieving this goal (Mcleod et al., 2011) and a potential carbon source if further habitat degradation is not avoided (Macreadie et al., 2014).

Soil organic carbon pools have only recently been recognized for their contributions to mitigating global climate change (Chmura et al., 2003 ; Laffoly & Grimsditch 2009 ; Donato et al., 2011 ; Fourqurean et al., 2012 ; Howard et al., 2014). Most estimates of carbon storage by seagrasses are based on the first 1 m of soil wherein up to 85% of seagrass biomass may reside (Fourqurean & Zieman, 1991) and do not account for deeper soils despite their comparatively large carbon pools (Pendleton et al., 2012). Measurement of soil carbon pools is typically accomplished by taking a statistically significant number of vertical cores and processing for soil depth, dry bulk density, and percent organic carbon content (Howard et al., 2014). While spectral methods exist for remotely predicting soil organic carbon content in terrestrial systems (Dalal & Henry 1986 ; Gomez et al., 2008), no such remote applications exist for aquatic systems. Global estimates of carbon in SAV soils are based on a limited number of habitats (Serrano et al., 2014), highlighting the need for more efficient, continuous sampling techniques required to assay larger volumes of soils across many aquatic habitats.

The flooded nature of submerged soils associated with seagrass beds may provide useful direction in generating new methods for measuring soil organic carbon content. Previous work

has demonstrated that regardless of soil origin, organic carbon and dry bulk-density exhibit a strong inverse correlation in flooded soils (Avnimelech et al., 2001). These results were upheld in studies of soils of seagrass meadows which showed increased organic carbon content and reduced mean dry bulk-density as the depth of sediment increases (Fourqurean et al., 2012). In this way if bulk-density of seagrass sediments or other characteristics such as porosity may be remotely identified, for example through acoustic surveying, the organic carbon content of these soils may also be indirectly estimated.

Acoustic studies of seagrass sediments are largely limited to shallow substrate composition (Munday et al., 2013), surface sediment grain size (De Falco et al., 2010 ; Micallef et al., 2012), or surface sediment type (Jordan et al., 2005 ; Warren & Peterson 2007). While these studies are useful for surveys of surface characteristics, they do not provide data on deeper sediment layers where carbon is sequestered. For measurements of soil carbon pools in seagrass to be useable, acoustic surveying methods should capture high-carbon content soil bands in at least the first 1 m of sediment as has been sampled in other studies (Pendleton et al., 2012). To date only two acoustic studies of seagrass meadows (one unpublished) appear to have captured this depth range (Pergent et al., 2015 ; Lo Iacono et al., 2008). While acoustically informative, both studies were performed in beds of matte-forming *Posidonia oceanica*, which is not physiologically representative of the many seagrass species which do not form mattes yet also contribute to soil carbon pools (Pergent et al., 1994). The work of Lo Iacono et al. (2008) also did not observe discrete layers associated with high-carbon content, but instead estimated the volume of the entire detritus matte deposited over time and subsequently inferred total organic carbon content. Further research is needed to expand acoustic surveys into non-matte forming

species and to provide methods for the measurement of high-carbon content layers within a continuous soil matrix.

Unlike traditional sub-bottom profilers (SBP) which may utilize single-beam transducers, parametric, non-linear SBP such as that used by Lo Iacono et al., (2008) simultaneously generate two waves at frequencies which interact to produce a single, high sound pressure wave at very low frequency (Innomar). For example, in this study the parametric echosounder generated a primary wave at 100 kHz and a secondary wave at 115 kHz, which interacted to produce a difference wave at 15 kHz. The resultant low-frequency wave features minimal side-lobes, allowing improved centimeter-scale vertical resolution of buried targets when compared to traditional linear acoustics (Wunderlich et al., 2005).

A study site approximately 52,000 m^2 was selected from the Lower Laguna Madre (LLM) of South Texas - a large bay of shallow seagrass meadows with an average depth of 75 cm (Quammen and Onuf, 1993). The LLM represents 80% of all remaining seagrass habitat in Texas (Blankenship, 2006), and is largely dominated by dense beds of *Thalassia testudinum* peppered with bare patches of sediment ranging from < 1 m^2 to over 85 m^2 (Greene et al., 2017 - unpublished). Depths in the study site averaged approximately 0.8 m. The selected area was chosen for its variety in cover (thick seagrass beds interspersed with bare sediment patches), having a gradient of anthropogenic stress (high levels of physical disturbance in some areas), and for ease of access.

Methods

Parametric Data Collection

In this study an Innomar "SES-2000 Compact" parametric echosounder (Innomar Technologie, Rostock, Germany) was utilized for all surveys, operated at a secondary wave frequency of 15 kHz to maximize vertical resolution within the first 1 m of soil. All available frequencies on the SES-2000 Compact were tested *in-situ* and 15 kHz was selected for its improved vertical resolution within the first 1 m of sediment compared to lower frequencies. Lower frequencies tested showed no significant improvement of penetration through areas of dense seagrass compared to 15 kHz. Sonar recordings were recorded in the Innomar SESWIN application and corrected for ship motion in real-time using a Ship Motion Control inertial measurement sensor (Part# IMU-108-30). GPS position was recorded using a DigitalYacht GPS-150 USB WAAS-enabled GPS+GLONASS receiver which was connected to the laptop used for data capture (Dell Latitude E6540 running Windows 7).

Two types of parametric samples were collected for this study: continuous moving acoustic transects, and stationary acoustic samples. Continuous transects consisted of 6 North/South transects spanning the entire length of the study site spaced 20 m apart, and 21 East/West transects crossing over the site spaced 30 m apart (Appendix F). Stationary acoustic samples were collected at 23 sites from the study area and randomly selected so 12 fell on seagrass beds and 11 fell on bare patches. All stationary acoustic samples were 60 seconds in duration. The 6.4 m survey vessel was secured prior each stationary acoustic sampling with two stern-mounted "PowerPole" shallow-water anchors and a 2.5 cm diameter metal rod hammered into the sediment before being secured with rope to a port-side cleat. To minimize vessel movement no crew moved during the 60 second duration of stationary acoustic sampling. Soil

cores were taken directly under the parametric transducer immediately after the acquisition of stationary acoustic samples. Continuous transect data would be used to test if a moving vessel influences the detection of fine sediment layers through seagrass or through bare sediment patches, and similarly tested for whether these reflectors correspond to sediment characteristics observed in soil cores. A continuous map of soil organic carbon can potentially be produced for the study site based on observed soil core characteristics and their association to corresponding reflectors in parametric recordings.

Laboratory test of parametric sonar

A brief laboratory test of parametric sonar's ability to differentiate fine sediment layers was conducted wherein a large plastic tub (0.71 m^3 capacity) was placed on insulating foam pads and filled with a layer of sand approximately 10 cm in height (Fig. 18). A 10 cm thick layer of fine sediments collected from local bay seagrass beds, having been dried in the sun for several weeks, was then deposited on top of the sand layer. To avoid mixing, thin tissue paper was layered on top of the sand layer prior to placing seagrass sediments. Post-test observations confirmed the tissue paper layer dissolved after sediment saturation. The tub was filled with local seawater and the parametric transducer suspended approximately 50 cm above the seagrass sediment layer top. Readings were collected at 15 kHz to provide proof of concept that parametric sonar can detect layering within a simplified soil matrix in shallow water conditions. It was determined that under laboratory conditions and a simplified soil matrix, parametric sonar operated at 15 kHz was capable of detecting an boundary between two sediment layers in shallow water conditions (Fig. 19).

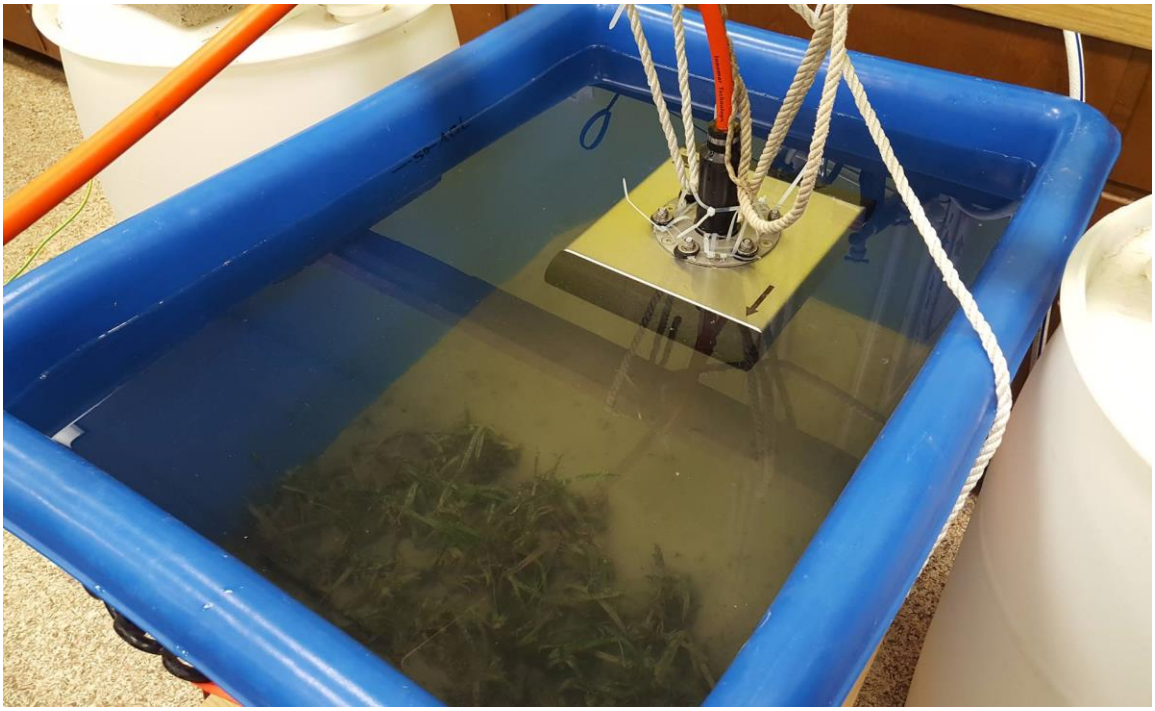

Figure 18, photograph of the laboratory parametric test wherein a large tub was filled with two 10 cm layers of sediment with differing porosity (seagrass sediments and sand) and sampled with a parametric transducer suspended 50 cm above the sediment surface.

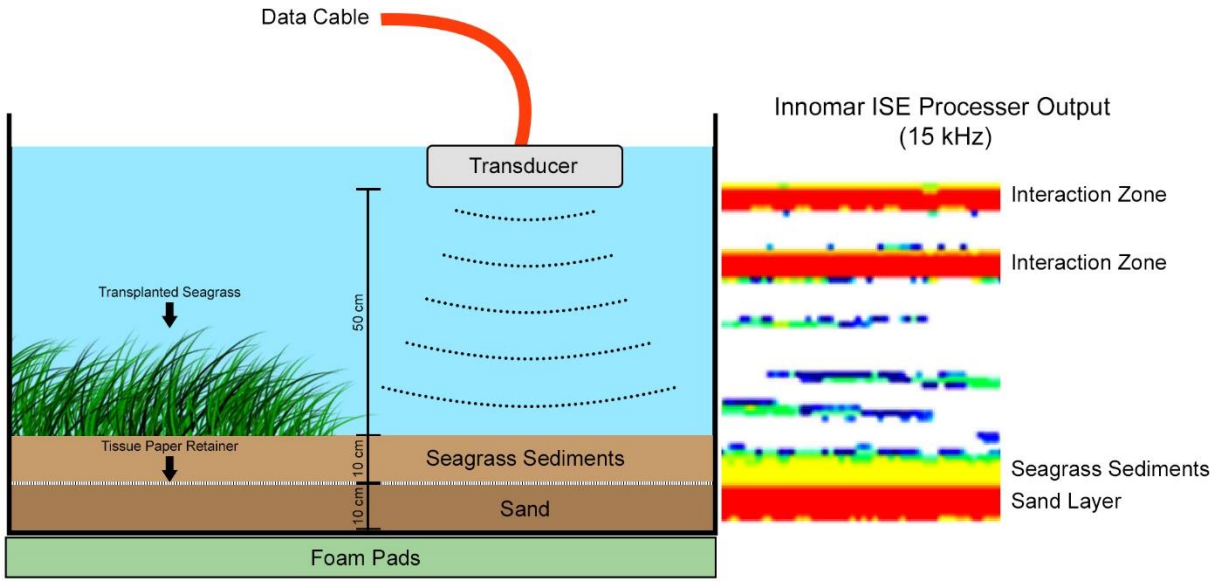

Figure 19, experimental set up and parametric sonar output from a laboratory test which placed a transducer approximately 50 cm over a two-phase simulated seabed containing two 10 cm layers of sediments with differing grain size. These results provided proof of concept that the Innomar Compact 2000 array can detect sediment layering in very shallow water depth (< 1 m) under idealized conditions.

Soil Core Field Collection

A total of 23 soil cores were collected within the 52,000 m^2 plot. Each core was taken directly underneath the parametric transducer immediately following stationary acoustic sampling, resulting in 12 cores taken from seagrass beds, and 11 cores taken from bare sediment patches. Twelve of the 23 total cores (6 bare, 6 seagrass) were collected in late summer (August), and another 11 (5 bare, 6 seagrass) in early winter (November) to represent phases for both seagrass growth and senescence. Soil cores measured 1 m long, and captured an average column of soil measuring 85 cm from the sediment top. Coring tubes were constructed from 1 m long PVC (thickness: 2 mm, inside diameter: 7.7 cm) and featured an open top to avoid compression during insertion. Cores were inserted via hammering with a large sledge hammer, a thick PVC T-junction was placed on top of the coring tube to allow venting of water and provide a large surface to strike while driving the core. After the core reached its target depth, the T-junction was removed and the core top was sealed with a 7.6 cm polyurethane cap (U-LINE, Pleasant Prairie, Wisconsin USA) and secured with a hose clamp. A winch and ladder were used to raise sealed cores while shovels, trowels, and PVC probes were used to break any seal of surrounding sediments to the outside of the core tube. Cores were raised the last 30 cm by hand, and the bottom was sealed with a hand prior to removal to avoid loss of sediment. Immediately following core extraction the open bottom end of the core tube was capped with a U-LINE brand 7.6 cm polyurethane cap and secured with a hose clamp to produce an air-tight seal. Sealed tubes were kept upright (sediment top up), covered from sun exposure, and transported from the field site on a foam cushion to minimize mixing vibrations. Cores were kept on the vessel for no more than 5 hours over the course of the field day before transport to the lab and immediate freezing in an upright freezer at approximately -17 °C.

Soil Core Processing

Once completely frozen, PVC tubes complete with core sediments inside were sectioned from the sediment top at 5 cm increments using a miter saw and composite blade. This process produced an average of 17 disks per core which averaged 4.64 cm thick after cutting. These 17 disks effectively represented subsections of the soil profile from the sediment surface to an average depth of 85 cm. Disks were labeled by core and numbered corresponding to disk depth. All disks were weighed, and placed in an oven at 65 °C until completely dry (~ 5 days). Dried disks were weighed and the tube volume calculated (based on disk inside diameter and four orthogonal measurements for disk height). Based on these metrics the dry bulk-density for each disk was calculated. Features such as shells and roots were left in samples so that bulk-density measurements would represent the "acoustic" bulk-density of the soil at a given depth – i.e the actual density of the substrate a sound wave is interacting with at a given point in the soil profile. Gradients of dry bulk density and porosity at each disk subsection would later be compared to the acoustic response at corresponding depths to investigate if soil properties may be used to inform acoustic response within the soil profile. Any disk data which may have been missing in a core, such as the bottom disk sediments being lost during collection, was back-filled using averaged data from the same disk number in all other cores of similar cover (seagrass or bare). After filling missing disk data all cores extended from 0 to at least 90 cm into the sediment.

Protocols described in the 2014 Coastal Blue Carbon methods manual were used to assay soil organic carbon content (Howard et al., 2014). Dry disk contents were individually pulverized with a mortar and pestle until uniform and sifted to a maximum particle size of 120 mm. Sub-samples weighing 0.5 g of each disk's material were ashed in a muffle furnace for 4 hours at 500 °C to remove organic carbon. Both ashed and uncombusted soil samples (4 – 6 mg) from each

disk were then ran through a CHNS Elemental Analyzer (PerkinElmer, Waltham, Massachusetts, USA) to acquire percent inorganic and percent total carbon, respectively. Organic carbon content was calculated following Table 3.5 from Howard et al., (2014) (Table 1). These assays provided a vertical profile of both bulk density and soil organic carbon content for each core at increments of 5 cm for the first 90 cm of sediment. Profiles were generated for each individual core and averaged to produce generalized soil profiles for both seagrass and bare patches. For all depth intervals in each core total kg organic carbon was calculated for a 1 m^2 area with height 5 cm (Equation 5). Porosity was calculated as the ratio of sample water volume (via mass lost during drying) to total disk volume.

$$5.\ \text{kg OC per m}^2 = (1\ \text{m}) \times (\text{Disk Height}) \times (\text{Dry Bulk Density}) \times \frac{\%\ \text{OC}}{100} \times 1000$$

Table 1, equations utilized to determine organic carbon content of soil samples. Adapted from Howard et al., 2014.

Sample ID	**Total Carbon Content (Elemental Analyzer)**	**Dry Mass Before Ashing (mg)**	**Dry Mass Before Ashing (mg)**	**Inorganic Carbon Content of Ashed Sample (Elemental Analyzer)**	**Inorganic Content of Sample**	**Organic Carbon Content of Sample**
	A	B	C	D	E = D × (C/B)	F = A - E
Example	25%	500	250	10%	5%	20%

Parametric Data Processing

Processing of parametric data differed for continuous or stationary data files. Stationary files were imported into the Innomar ISE processing package (Innomar Inc.) and the 15 kHz low-frequency channel from each file processed to produce a single signal trace consisting of 480

returns for the first 4 m of soil sediments, averaged across the entire 60 second recording. Due to a lack of information covering sound propagation in seagrass sediments, a uniform sound speed of 1560 m/s was assumed for both the water column and sediment returns. Signal traces were classified as having been collected over seagrass or bare sediment, and return amplitude plotted alongside sediment profile data to investigate if any associations existed between soil characteristics and acoustic envelope return strength.

Continuous parametric files had both high-frequency (100 kHz) and low-frequency (15 kHz) data channels imported into the Innomar ISE processing package. High-frequency files underwent a 5 pixel smoothing window, an automated median filter to reduce noise, and were processed to leverage the improved vertical resolution of the 100 kHz wave to emphasize visibility of the seafloor through the seagrass canopy. Low-frequency files were processed with a 10 px smoothing window, automated median filter to reduce noise. The high vertical resolution of the high-frequency data was used to establish the seafloor, while the high penetration of the low-frequency wave was used to identify layers within the sediment if present. After processing all continuous files were exported from the Innomar ISE package and imported into SonarWiz 6 (Chesapeake Technologies Inc) for plotting, bottom-tracking, and identification of acoustic reflectors.

Results

Soil Cores and Sediment Profile Characteristics

Metrics for dry bulk density, porosity, percent organic carbon, and kg organic carbon per m^2 were generated from collected soil cores & compared with a Welch's T-Test. Profiles within either seagrass or bare patch sediments were found to be consistent, with very little variation

across the 52,000 m^2 sample area. As bare patch areas mostly or completely lack the soft upper sediments accrued by seagrass meadows, all bare patch cores were shifted downwards by 5 cm in all analyses. The shift allows data from the top section of the sediment core (section #1, top 5 cm depth) in bare patches to be compared to the section #2 of sediments (10 cm depth) in the seagrass meadows. Dry bulk density was both highly similar between seagrass and bare patch sediments across the full soil core range, with significant differences only occurring in disks at 70 cm ($p = 0.011$, $df = 17$). (Fig. 20). Soft sediments found in about the first ~5 cm of vegetated areas and absent from bare sites featured low bulk density with a mean value of 0.33 g / cm^3. Porosity in vegetated sediments were significantly different from unvegetated sediments only at 70 cm ($p = 0.024$, $df = 19$) and 90 cm ($p = 0.033$, $df = 20$). Sediments lost from the tops of bare patches but present in vegetated areas featured a mean porosity of 0.73. Porosity and bulk density were inversely associated for all disks in all cores (Fig. 21).

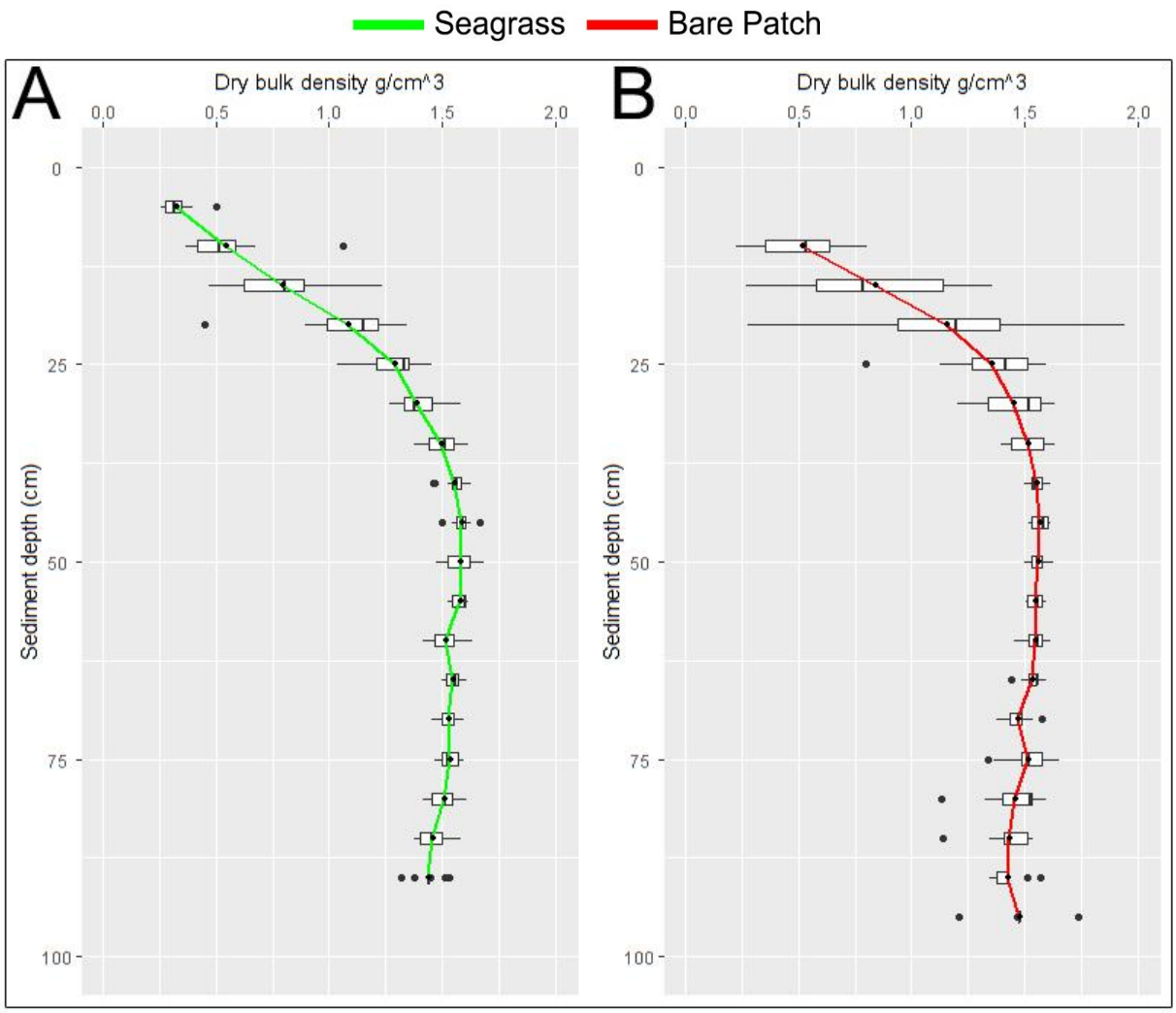

Figure 20, box plot and mean lines representing dry bulk density as a function of depth for cores taken in both vegetated (seagrass) and unvegetated sediments (bare patches).

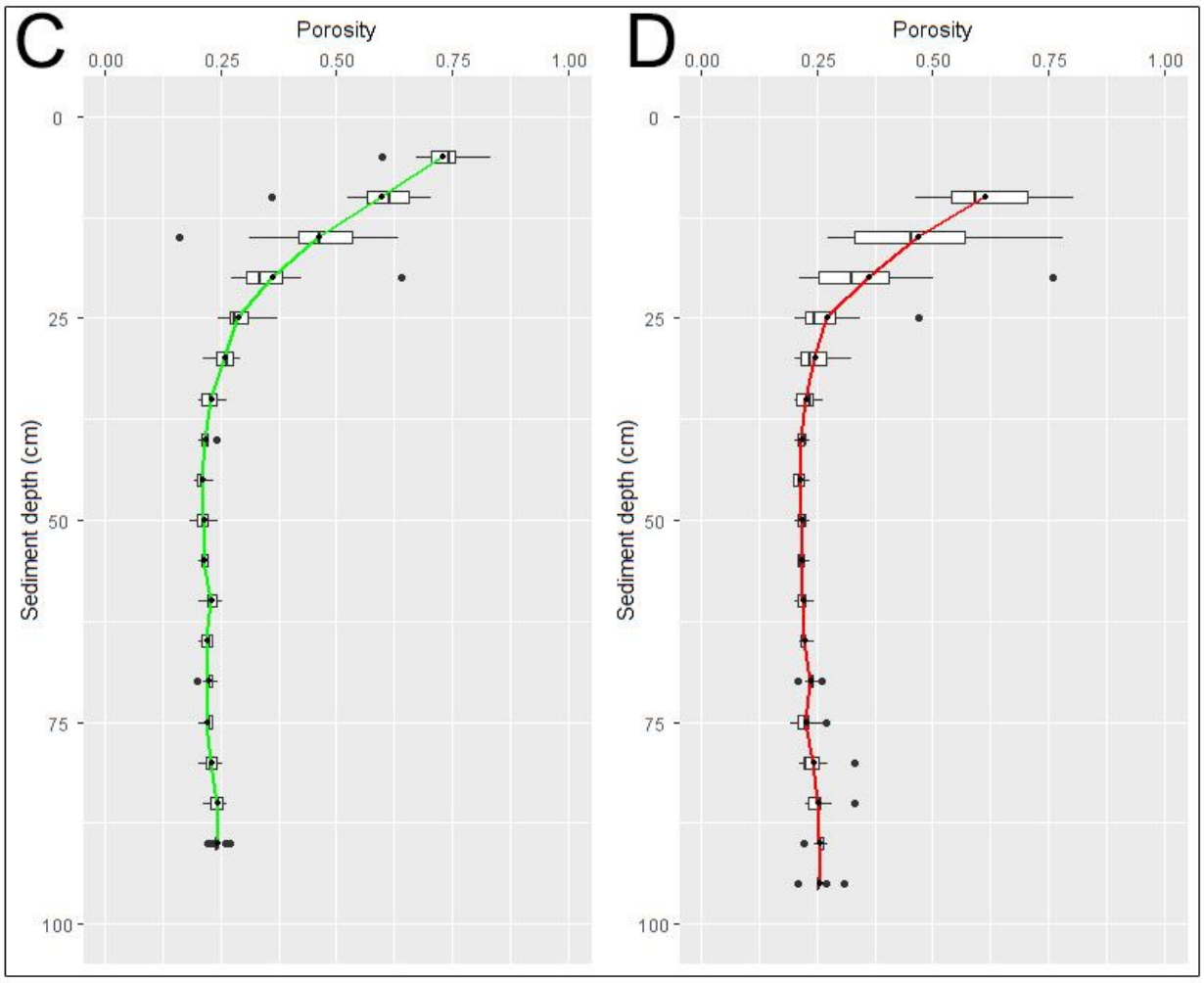

Figure 21, box plot and mean lines representing porosity as a function of depth for cores taken in both vegetated (seagrass) and unvegetated sediments (bare patches).

Percent organic carbon was high (mean 4.71 %) in the soft top 5 cm of seagrass sediments, and decreased with increasing depth and stabilizing near 0.50 % in sediments deeper than 60 cm (Fig. 22). Beyond the top layer of soft carbon-rich soil seen in vegetated areas, sediments present in both seagrass and bare cores only differed significantly at the 35 cm disk ($p = 0.028$, $df = 19$). In all core sediments shallower than ~ 50 cm percent organic carbon exhibited a strong direct correlation with porosity, and a similarly strong inverse correlation with dry bulk density. Beyond ~ 50 cm, no clear relationship to either porosity or dry bulk density was observed. (Fig. 23, Fig. 24).

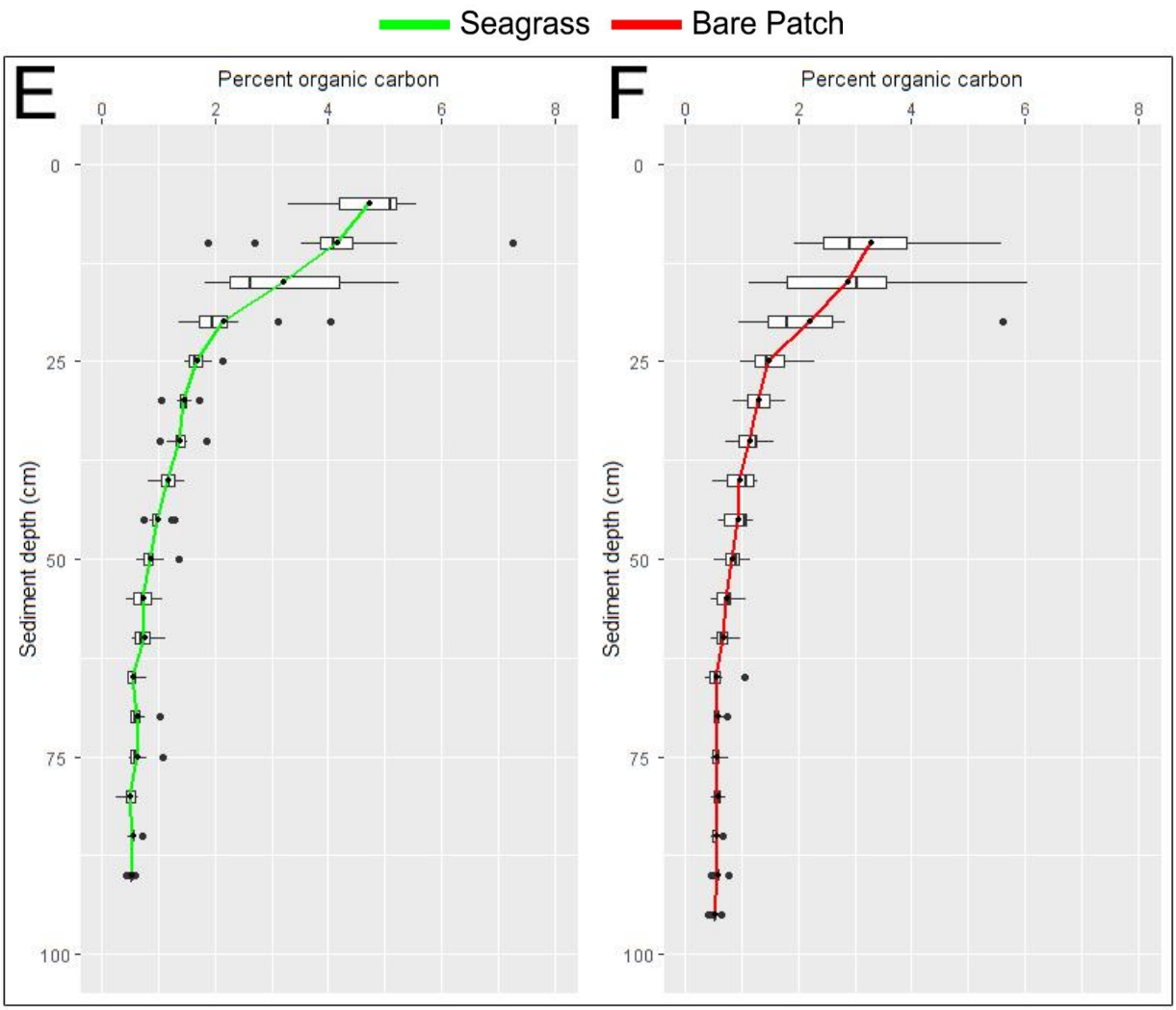

Figure 22, box plot and mean lines representing percent organic carbon as a function of depth for cores taken in both vegetated (seagrass) and unvegetated sediments (bare patches).

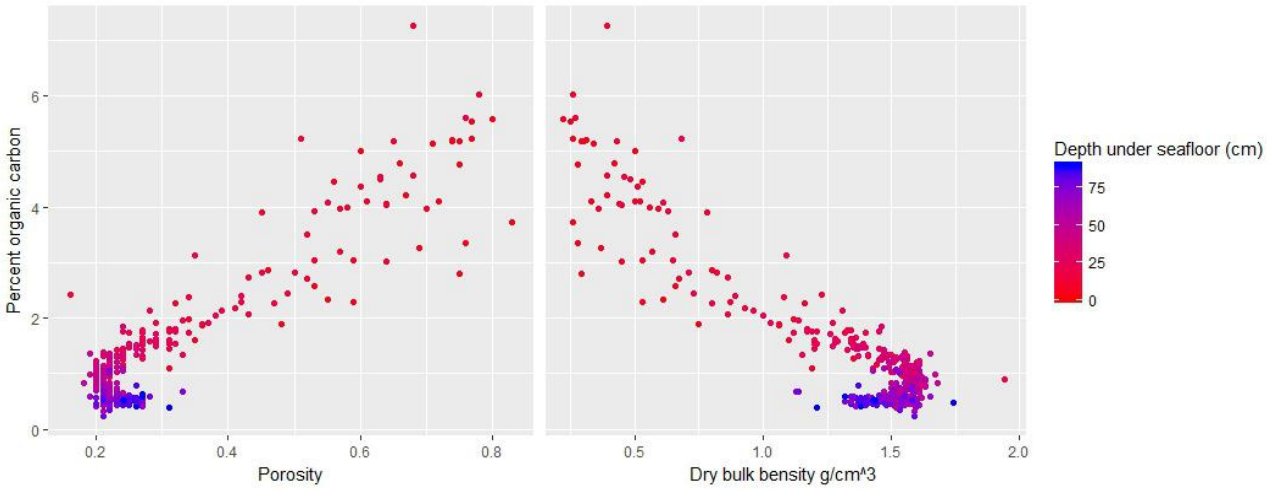

Figure 23, percent organic carbon from sediment depths 0 – 90 cm as a function of either porosity or dry bulk density for all soil cores collected in the study site.

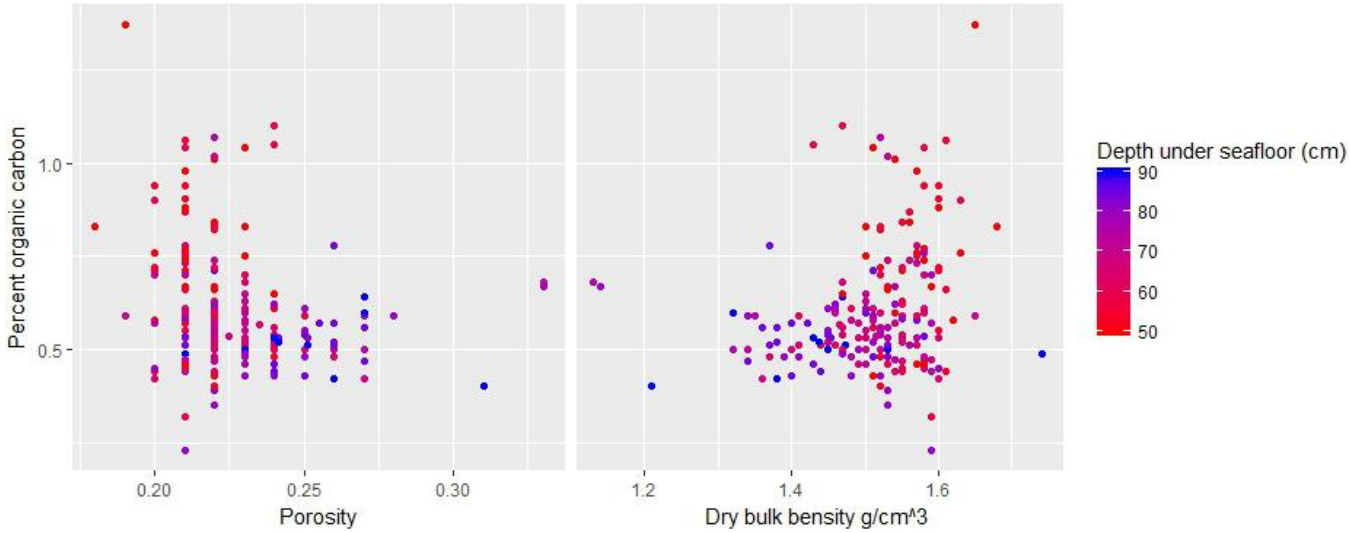

Figure 24, percent organic carbon from sediment depths 50 – 90 cm as a function of either porosity or dry bulk density for all soil cores collected in the study site.

Total weight organic carbon (kg OC m^2) was measured both for individual depth increments and as an accumulation upwards from 90 cm to the seafloor. Despite having the highest percentage of organic carbon, the top 5 cm of low-porosity sediments seen in vegetated areas and absent from bare patches did not contain the most total organic carbon by weight in seagrass cores. These sediments averaged 0.76 kg OC m^2, yet sediments contributing the most carbon by weight occurred at a depth of 15 cm (1.09 kg OC m^2) in vegetated cores. Unvegetated

sediments displayed similar characteristics, with layers approximately 20 cm below the seabed carrying the most carbon by weight on average (1.02 kg OC m^2) (Fig. 25). Comparisons of seagrass cores to bare patch cores showed significant differences in carbon content by weight at disks for 10 cm ($p = 0.011$, $df = 18$), 25 cm ($p = 0.045$, $df = 19$), and 35 cm ($p = 0.013$, $df = 19$).

Bare patch cores averaged a total accumulation of 11.10 kg OC m^2 between 10 and 90 cm, while seagrass cores averaged 12.28 kg OC m^2. Seagrass core total accumulated carbon averaged 13.04 kg OC m^2 if including an additional top 5 cm of soft sediments (Fig. 26). Seagrass cores with top sediments included had significantly increased total organic carbon (14.88%) over bare patch cores ($p = 0.012$, $df = 18$). When excluding soft top sediments, differences of total organic carbon content in bare patch cores and seagrass cores was not significant for sediments from 10 – 90 cm ($p = 0.108$, $df = 18$). These soft ~5 cm of upper sediments make up 5.86% of total organic carbon to a depth of 90 cm in seagrass cores. Overall results suggest bare patches located within vegetated areas represent a reduced state of carbon storage compared to the surrounding seagrass meadow, and that this reduction is significantly associated with the loss of soft upper sediments.

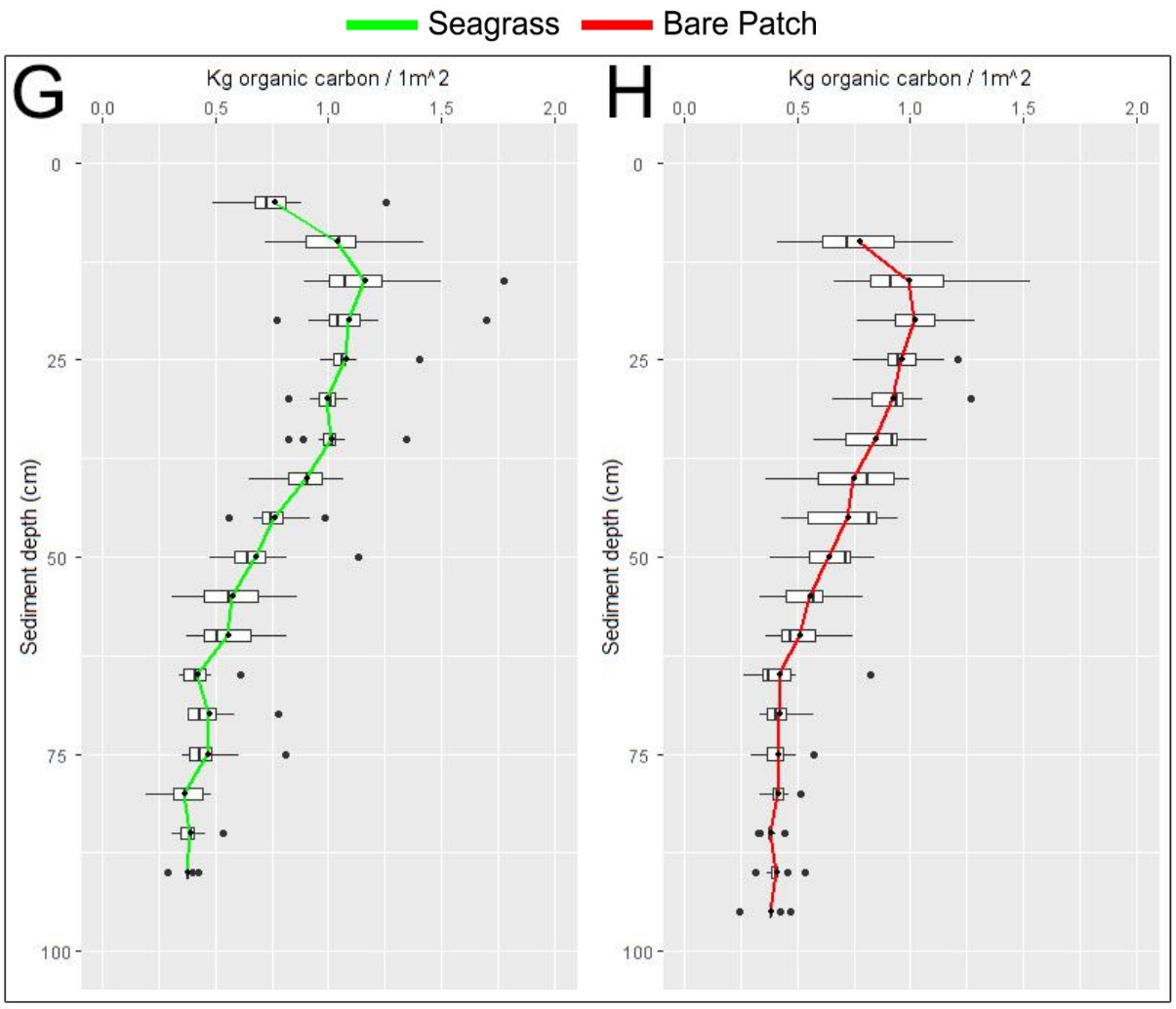

Figure 25, box plot and mean lines representing total organic carbon by weight as a function of depth for cores taken in both vegetated (seagrass) and unvegetated sediments (bare patches).

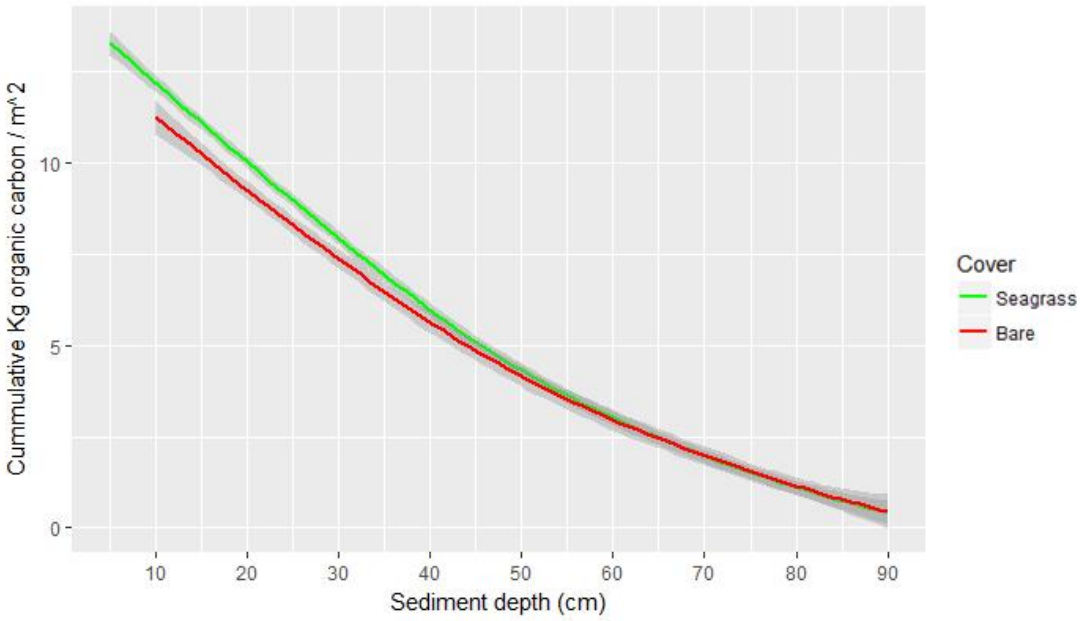

Figure 26, cumulative total organic carbon by weight observed across all soil cores taken in both vegetated (seagrass) and unvegetated sediments (bare patches), accumulated from 90 cm upwards to the sediment top. Grey area indicates 95% confidence interval.

Identifying corresponding layers in acoustic and soil core data

Bare patches with a clearly defined sediment-water interface (seafloor, n = 31) were selected from six continuous 600 m transects spanning the length of the study site at 20 m intervals. At least four distinct acoustic reflectors were visible in all 15 kHz parametric recordings taken over bare patches, spanning depths between 0 and 90 cm below the seafloor. Only the first four strong reflectors were utilized for this study to maintain a sediment depth range consistent with collected soil cores. Reflectors 1 through 4 corresponded to average depths of 24.1 +/- 2.5 cm, 38.7 +/- 3.61 cm, 56.6 +/- 4.6 cm, and 75.3 +/- 5.4 cm below the seafloor (Fig. 27). Parametric recordings taken over the same bare patch at different times and directions of travel also indicate that reflectors can be reliably observed across multiple surveys (Fig. 28). No discernable layering was visible in parametric recordings taken over seagrass. This result is

consistent with the documented strong attenuative properties of aerenchyma gaseous tissues present in seagrass and other macrophytes which act to slow the speed of sound waves, often to dispersive effect. Only bare patch soil cores (n = 11) were used to validate layering observed in bare patch acoustic samples.

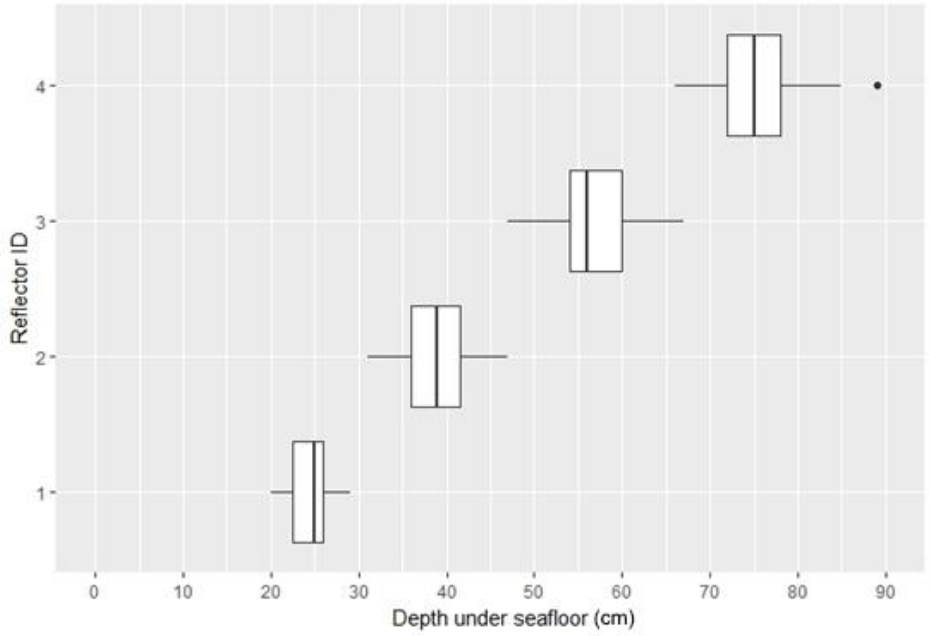

Figure 27, box plot of observed sediment depths for four distinct reflectors observed across 31 parametric recordings taken over bare patches with a clearly visible seafloor.

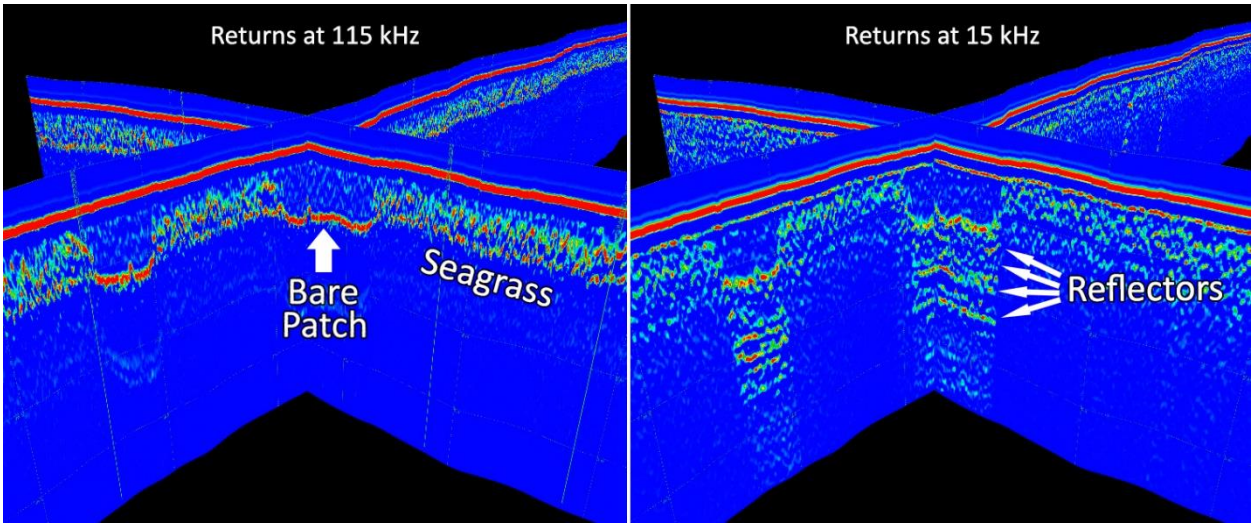

Figure 28, demonstration of a bare patch and associated seabed reflectors observed in separate orthogonal parametric transects. Observed depth of reflectors is conserved across both recordings suggesting reproducibility in parametric readings. No clear reflectors are visible under areas of seagrass immediately adjacent to the bare patches.

Porosity of sediments has well documented correlations to sound velocity and is one of the primary factors driving parametric interpretation of layer position in the seabed (Oelze et al., 2002 ; Ramakrishnan, 1994). Porosity also exhibited a strong direct correlation to organic carbon content in the study site and was found to be highly similar across the soil profile in both vegetated and unvegetated areas. To investigate if the depth of Reflectors 1 – 4 were associated with porosity changes in the soil profile gradient of porosity as a function of depth was averaged by disk for all eleven unvegetated soil cores. Comparing peaks in these plots (indicating sudden changes in porosity) to acoustic response would determine if associations of acoustic response to porosity of sediments in a seagrass habitat were present, and moreover, if these associations could be used to infer reflector position in surrounding seagrass sediments. Inflection in the study site's porosity gradient indicate as many as seven changes in soil porosity over the averaged profiles of 11 unvegetated cores (Fig. 29).

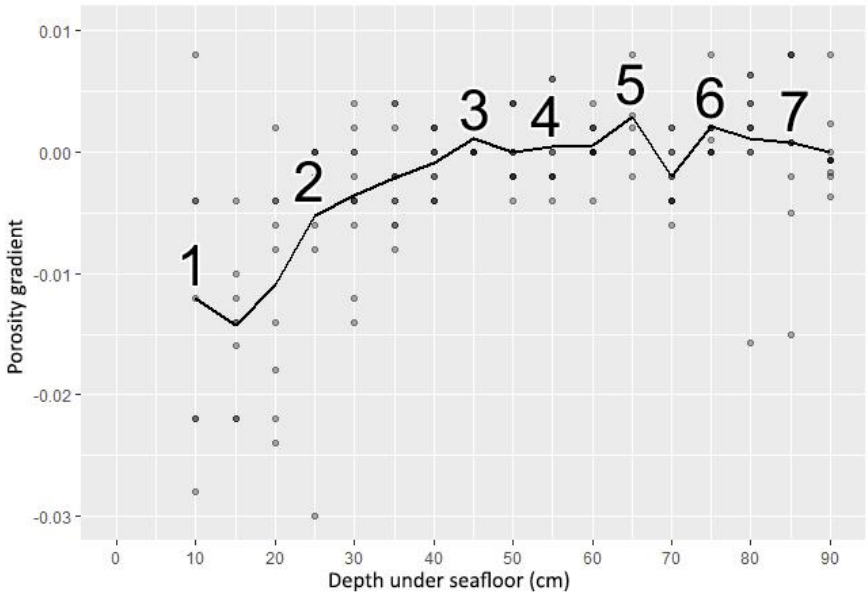

Figure 29, porosity-gradient for all unvegetated cores is plotted every 5 cm with 30% transparency to allow for overplotting of points. Darker points indicate identical results across several cores. Also included is a curve for mean porosity-gradient across all unvegetated cores for all depth intervals to demonstrate overall trends in the change of porosity as a function of depth across the study site. Previous studies of porosity and sound speed would suggest parametric reflectors may associate with one or several of these porosity inflection points.

The relationship of sediment porosity to sound speed would suggest that reflector position in a vertical column of soil may be associated with changes in soil porosity. When comparing recorded depths of the four observed reflectors seen throughout the study site, several of the acoustic reflectors appear strongly associated with visible changes in porosity gradient (Fig. 30). Reflector 1 appears strongly associated with porosity-gradient maxima 2 at approximately 25 cm sediment depth. Reflector 2 does not appear to be associated with any particular porosity-gradient maxima, and may represent influences on acoustic response by additional soil characteristics. Reflector 3 appears strongly associated with a small change in porosity visible at approximately 55 cm sediment depth. Reflector 4 also appears strongly associated with a change in porosity at approximately 75 cm sediment depth. Tests for similarity

of porosity between vegetated and unvegetated sediments at each 5 cm depth interval indicate no significant differences between these soil profiles up to 70 cm depth. Only the 70 cm ($p = 0.024$, $df = 19$) and 90 cm ($p = 0.033$, $df = 20$) disks were found to be significantly different in vegetated or unvegetated sediments. These results suggest that reflectors 1 and 3, which reside above 70 cm and are closely associated with changes in porosity, may be inferred into vegetated areas if present in nearby bare patches.

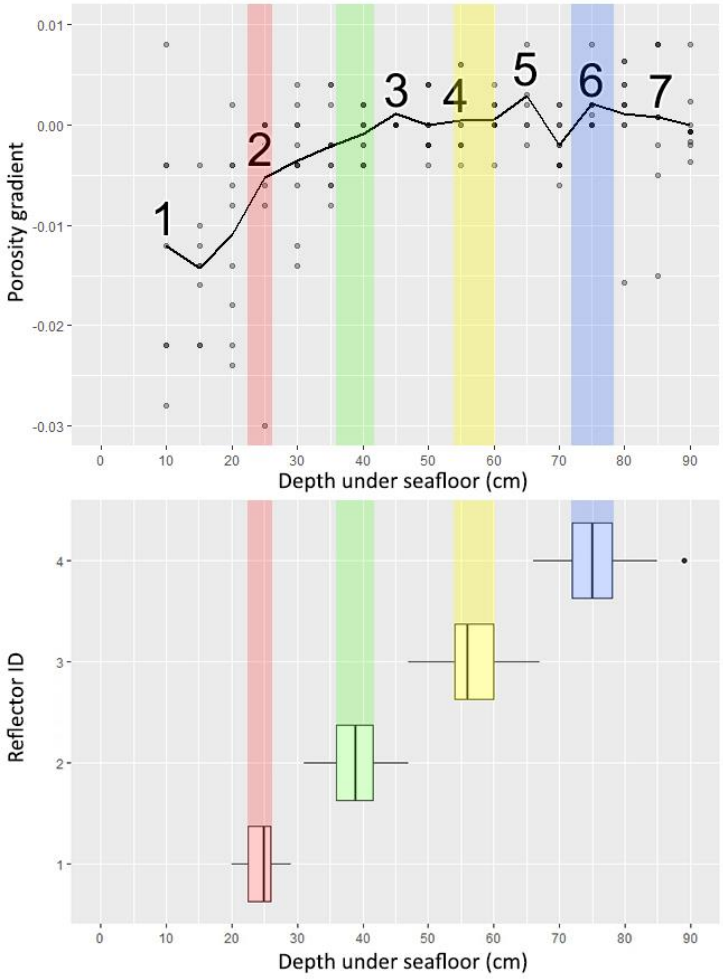

Figure 30, demonstration of alignment between acoustic reflectors observed under unvegetated sediments and changes in porosity-gradient identified in unvegetated soil cores. Reflectors 1, 3, and 4 appear closely associated with changes in porosity observed at inflection points 2, 4, and 6 respectively.

A Spearman Rank correlation test was performed to determine if any statistical correlation existed between the position of a reflector in parametric returns, and the position of porosity-gradient inflection points within the soil column. Eleven bare patches sampled with parametric sonar were randomly selected from the 31 total sample sites, and the depth of their reflectors compared to corresponding inflection points in porosity-gradient (e.g depth of reflector 1 across all 11 randomly chosen bare patches compared to depth of porosity gradient 2 in all 11 bare sediment cores). Reflector depth values were rounded to the nearest 5 cm increment to match the resolution of soil core data used in the test. Reflector 1 had a significant correlation to porosity changes at porosity-gradient point 2 ($r(9) = 0.53$, $p = 0.047$). Reflector 2 was not found to be significantly correlated with porosity-gradient point 3 ($r(9) = 0.51$, $p = 0.053$). Reflector 3 was strongly correlated with changes in porosity occurring at porosity-gradient point 4 ($r(9) = 0.76$, $p = 0.003$). Reflector 4 was not significantly correlated with porosity-gradient point 5 ($r(9) = 0.51$, $p = 0.054$).

Using reflectors to estimate carbon content of vegetated areas

Mean sediment depth (MSD) of reflectors observed in parametric transects may be combined with soil core profiles of total organic carbon content to provide an estimate of the total carbon associated with sediments occurring above each reflector. These estimations may be calibrated for areas of bare sediment or currently vegetated areas by including or excluding those disks which represent the first 5 cm of soft sediments seen only in vegetated areas. Soil profiles indicate sediments occurring between the seagrass seafloor and Reflector 1 (MSD 24 cm) amount to approximately 3.7 kg OC / m^2 in bare patches, and 5.1 kg OC / m^2 in vegetated areas. Sediment occurring between Reflector 1 (MSD 24 cm) and Reflector 2 (MSD 38 cm) contain

approximately 6.2 kg OC / m^2 in bare patches, and 8.1 kg OC / m^2 in vegetated areas. Sediment occurring between Reflector 2 (MSD 38 cm) and Reflector 3 (MSD 56 cm) contain approximately 8.1 kg OC / m^2 in bare patches, and 9.9 kg OC / m^2 in vegetated areas. Those sediments occurring between Reflector 3 (MSD 56 cm) and Reflector 4 (MSD 75 cm) contain approximately 9.9 kg OC / m^2 in bare patches, and 11.9 kg OC / m^2 in vegetated areas. Reflectors 1 – 4 approximately contain 33.7%, 56.2%, 73.4%, and 89.2% f the total carbon observed to an adjusted depth of 90 cm in bare patches, respectively. In areas of seagrass which contain an additional 5 cm of soft sediments Reflectors 1 – 4 approximately contain 39.0%, 61.4%, 76.8%, and 91% of the total organic carbon observed to a depth of 90 cm, respectively. Significant differences in porosity between bare patch sediments and equivalent sediments in vegetated areas were found for sediments at 70 cm ($p = 0.024$, $df = 19$) and 90 cm ($p = 0.033$, $df = 20$), suggesting the position of Reflector 4 may not be uniform across vegetated or unvegetated sites. Reflector 2 did not appear to be largely associated with changes in porosity, and was excluded from further analysis. Uniformity of porosity across vegetated and unvegetated sediment profiles may be taken as evidence that the depths of Reflectors 1 and 3 are consistent regardless of vegetation presence, and that Reflector 4 may not have consistent depth across these gradients. These results suggest assumptions of the total carbon associated with sediments above each reflector in seagrass areas may be made for Reflectors 1 and 3, for which corresponding sediments in seagrass and bare patches have similar carbon content and porosity.

Parametric transects and cross-transects produced a grid of approximately 52,415.06 m^2 with 120 total intersection points. Vegetated and unvegetated coverage of the grid area was calculated in ArcMap 10.3.3 using drone imagery collected on 23 August 2017 from an altitude of 100 m (resolution 4.51 cm / px). In total 49,346.15 m^2 was recorded as vegetated, and

3,068.91 m^2 as unvegetated (bare sediment). Cumulative averages of 11.10 kg OC / m^2 for bare sediment and 13.04 kg OC / m^2 were used to calculate total carbon content of the grid area to a depth of 90 cm. Including 5 cm of soft upper sediments in vegetated areas, the site's total carbon was estimated to be 643,473.80 kg organic carbon. Excluding the top 5 cm of vegetated soft sediments reduces total organic carbon to 605,970.72 kg indicating the soft upper sediments only found in vegetated areas may be responsible for as much as 37,503.08 kg organic carbon. The 3,068.91 m^2 of unvegetated sediments within the grid area which have lost their soft top sediments represent an approximate loss of 2,332.37 kg organic carbon.

Reflector 3 captured the largest sediment profile with a MSD of 56 cm beneath the seafloor in bare patches. Like the shallower Reflector 1, porosity of sediments associated with Reflector 3 (50 – 65 cm depth range) were not found to be significantly different between seagrass and bare patch areas – suggesting that the depth of Reflector 3 may be constant across both vegetated and unvegetated areas. The first 55 cm of bare patch sediments contained an average of 7.93 kg OC / m^2, while vegetated areas contained an average of 10.01 kg OC / m^2. For the entire 52,000 m^2 study site sediments captured by Reflector 3 (0 cm – 55 cm MSD) totaled 518,291.42 kg of organic carbon, approximately 76.50% of all organic carbon present in the first 90 cm of surveyed sediments.

Discussion

Parametric sonar has shown a distinct potential for the measurement of organic carbon associated with seagrass beds. Lo Iacono et al., (2008) demonstrated the ability of parametric sub-bottom profilers to detect a discrete transition from seagrass detritus matte to sediment. This work has expanded on Lo Iacono's 2008 research by demonstrating an indirect method of estimating the organic carbon content of sediments beneath a living seagrass meadow by

exploiting the patchy, heterogenous nature of these habitats. The findings suggest that parametric sonar is a feasible tool for estimating the contributions of seagrass carbon sequestration to a continuous soil matrix – a critical expansion from previous work which focused solely on a matte-forming seagrass. Parametric transects at low frequencies allowed the detection of reflectors at consistent depth in bare patches within a living seagrass ecosystem and across a large spatial scale. Attenuation and scattering of sound by seagrass gas-filled tissues did not allow our acoustic system to detect layers under living seagrasses. However, sediment cores taken in both vegetated and unvegetated sediments indicated no significant difference with respect to porosity to a depth of 70 cm. Acoustic reflectors at 25 cm, 56cm appear highly associated with changes in porosity-gradient, allowing the inference of these reflectors into surrounding seagrass-bed sediments with a similar porosity profile. It was found that the deepest reflector likely to be present in both vegetated and unvegetated areas captured on average more than 76% of the total organic carbon present in the entire 90 cm soil profile. Incidentally these measurements also allowed the estimation that the first 5 cm of seagrass sediments, those largely absent in bare patches, are responsible for 5.8% of the total carbon seen to a depth of 90 cm. Had this study taken cores to a depth of 55 cm these soft upper sediments would account for approximately 7.6% of the total organic carbon within the first 90 cm of soil.

To date it would appear this work is the second study to utilize parametric sonar in a seagrass habitat (following Lo Iacono et al., 2008), and only the third to acoustically investigate sediments beyond 50 cm in these habitats. Future research into the applications of parametric sonar for the survey of vegetated marine habitats should consider including a range of seasonality. Stationary parametric readings taken during this research during both September and November indicated strong attenuation. Reflectors visible in many November stationary readings

taken over bare patches were no longer visible in September stationary readings. Previous work by Wilson et al. (2013) demonstrated that the attenuative properties of seagrass canopies may be greatly diminished in periods of dormancy. While these results suggest sampling in dormant periods may limit attenuation by the seagrass canopy, recent work by Lee et al. (2017) has demonstrated that sediments below dormant seagrass remain highly attenuative compared to nearby bare sediments. Future work utilizing parametric sonar should balance these considerations to ensure the best chance of recording acoustic reflectors. One continuous transect recorded in February 2016 by the authors (15 kHz) did demonstrate improved perception of acoustic reflectors under dormant seagrass compared to those collected in September (Fig. 31). It would appear that this study may represent results of parametric sonar in sub-optimal conditions (very shallow water, and actively growing seagrass).

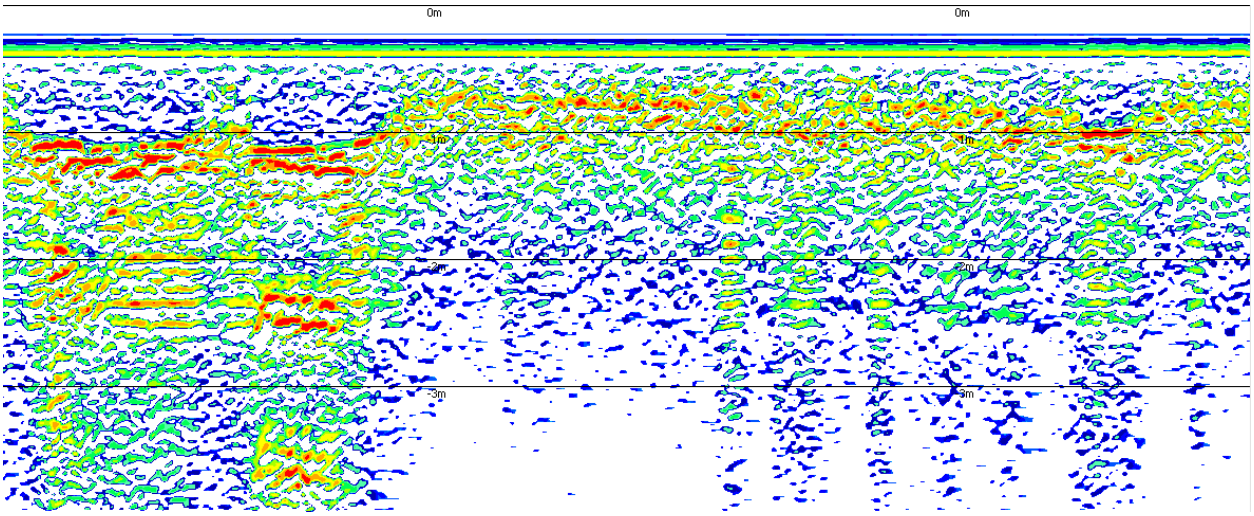

Figure 31, parametric transect at 15 kHz recorded in February 2016 (dormant period) while testing the Innomar system in a bed of *Thalassia testudinum*. Reflectors are clearly visible under bare sediment patches (left) and also partially visible under sparse seagrass meadow (center-right).

Many stationary parametric readings were taken for this study at coring sites, yet none yielded clearly visible reflectors at this time. Despite having been taken immediately prior to

collecting a soil core at all 23 core sites, stationary parametric readings demonstrated high variability across the study site – contrasting the relatively consistent soil profiles. This variability limited the utility of stationary readings for the detection of seabed reflectors, and would not allow for any statistical correlations of sediment characteristics to acoustic return strength in stationary readings. It is possible such variation occurred in part due to the survey vessel being very close to the transducer at the time of sampling. In a stationary setting it is possible the vessel's hull could have acted to produce irregular signal multiples over the time required to collect stationary samples and as the water column became increasingly saturated with sound from the transducers continuous transmissions. Future work may find it useful to place a parametric transducer on a tripod structure some distance away from the vessel before conducting stationary soundings. The author would also suggest further exploration into the correlation of acoustic return strength to soil characteristics such as sediment grain size *in-situ* as these associations have great potential to improve our interpretation of seabed reflectors in seagrass meadows and such studies are scarce in the literature.

A brief experiment was conducted to better understand whether seagrass blades or rhizome structures were responsible for a lack of reflectors under seagrass sites. Stationary readings were taken over areas of dense seagrass cover both before and after manual clipping of seagrass shoots to the sediment surface with careful attention to leave rhizome structure intact and not disturb surface sediments. Output from the parametric recordings appears to indicate improved signal penetration with blade removal, albeit with reduced performance compared to areas of bare sediment alone (Fig. 31). These findings would indicate both blade and rhizome tissues contribute to signal dissipation and could influence reflector recognition.

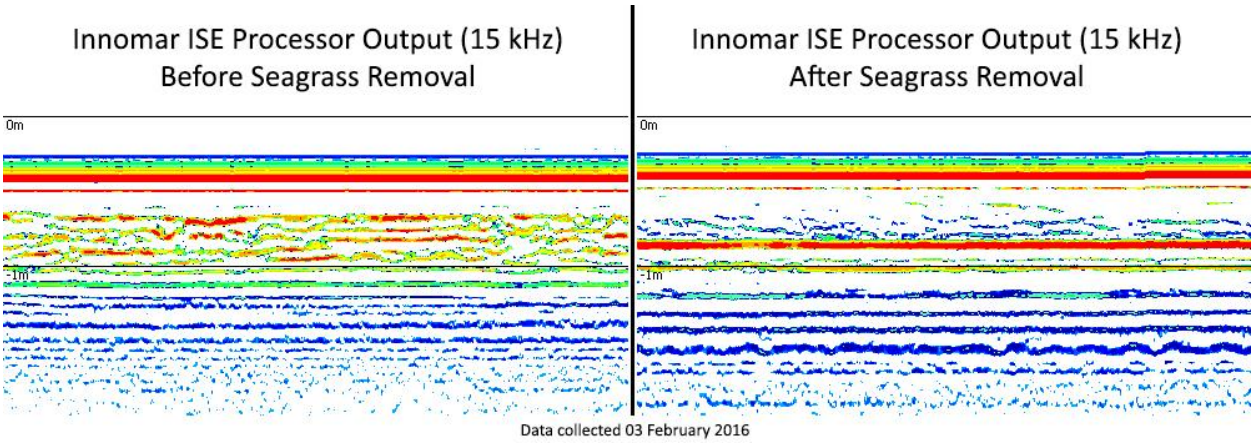

Figure 32, the results of a pilot experiment in which a patch of dense seagrass was sampled with parametric sonar (15 kHz) both before and after removal of seagrass shoots and blades. Signal penetration and recognition of reflectors is significantly improved in the absence of above-ground seagrass biomass.

An effort was made to use recorded parametric reflector depths observed under the study site to produce three-dimensional representations of either acoustic reflectors and the carbon content associated with them of the study site. Software packages such as SonarWiz 6 allow acoustic reflectors to be digitized with relative ease, and a three-dimensional surface to be generated by interpolating corresponding reflectors across multiple sonar files laid out in a fence diagram arrangement. Provided reflectors were not directly observed under seagrass areas and bare patches are not uniformly distributed, there may be significant error in the dimensions of these surfaces under vegetated areas. These surfaces represent a “best guess” of reflector position under vegetated sediments and can provide useful insights into the study of coastal ecosystems and their associated organic carbon such as the approximate volume of soil layers over large areas, or how soil organic carbon pools may spatially change based on surface vegetation coverage.

Five surfaces were generated from parametric recordings in SonarWiz 6. First a reference for the seafloor in absence of soft seagrass sediments was created by marking the tops of all bare

patches with a clear sediment-water interface and interpolating between them to create a complete surface. This process was repeated for Reflectors 1 – 4 found within the seabed. A native 3D viewer within SonarWiz 6 was used to visualize the resulting model of the study site (Fig. 33). Distance from seafloor (unvegetated sediment surface) to Reflector 3 was also calculated in ArcMap 10.3.3 to produce a map of soil profile thickness captured by Reflector 3 across the 52,000 m^2 study site (Fig. 34). While no direct measurements were made in these exploratory results, the potential for future research on the spatial extents of coastal soil organic carbon based on parametric reflectors is highly apparent.

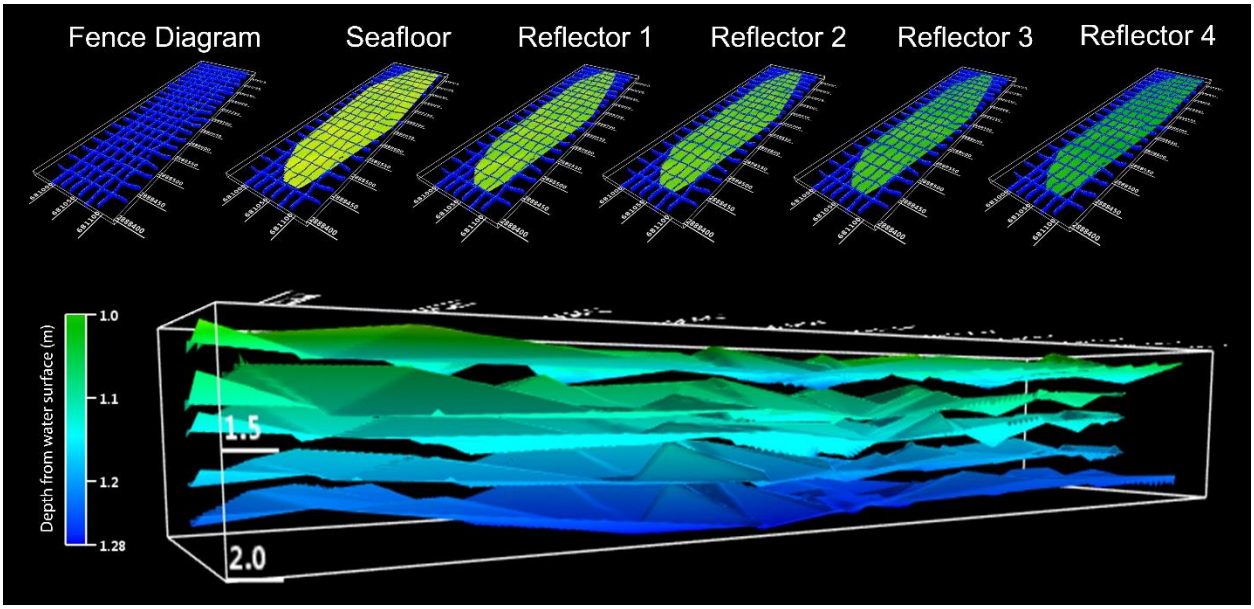

Figure 33, demonstration of the constructed fence diagram and three-dimensional surfaces for seafloor and Reflectors 1 – 4 observed under unvegetated sediments. All five surfaces were combined to provide a visual reference for reflector distribution across the study site.

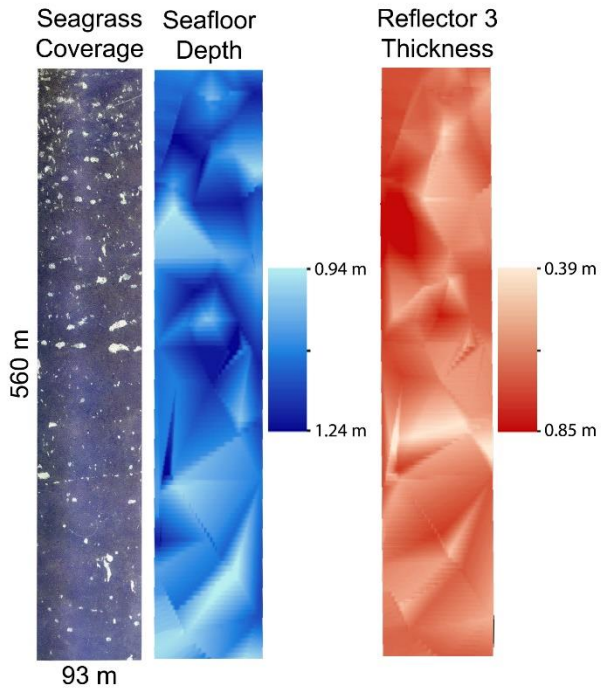

Figure 34, classified rasters generated in ArcMap 10.3.3 from three-dimensional surfaces based on reflectors observed under unvegetated sediments. Color grading indicates seafloor depth and thickness of sediments residing between Reflector 3 and the seafloor. A mosaic of drone aerial imagery is provided for seagrass coverage reference. Some error in soil profile thickness may be present due to extrapolation to raster boundaries (Inverse Distance Weighted) from sampled bare patches.

CHAPTER IV

OVERALL SUMMARY AND DISCUSSION

Seagrass meadows and similar sites of submerged aquatic vegetation continue to be recognized as globally significant in the capture and sequestration of atmospheric carbon. Seagrasses inhabit a proportionally small area globally yet capture more carbon than mature tropical forests, boreal forests, or temperate forests (McLeod et al., 2011). Despite valuations of ecosystem services rising to $1.9 Trillion, seagrass habitats are in global decline (Waycott et al., 2009). Methods used to study seagrass distributions at large scales have changed little over the past two decades, with most using randomized point surveys, satellite or aerial surveys, or acoustic echosounders to measure coverage. Methods to survey soil carbon pools enriched by seagrass are similarly limited, typically relying on soil cores which are both destructive and labor-intensive. New and more efficient methods to measure seagrass coverage and the distribution of organic carbon in shallow coastal ecosystems are required to inform discussions of the uncertain future these ecosystems face.

This work has introduced two independent methods for measuring two discrete metrics of seagrass habitats. We have presented methods by which an inexpensive, simple side scan array may be constructed from consumer-grade transducers and used to reliably measure coverage in a seagrass meadow. Additionally, the side scan chapter of this thesis has demonstrated that the constructed array is capable of functioning in coastal waters as shallow as 1 m while producing horizontal swaths up to 56 m. Shallow regions of seagrass growth are consistently

underrepresented in the literature, in part due to the inefficiency of using traditional acoustic instruments in such shallow conditions (multibeam, ADCP), and due to the meteorological limitations of satellite or aerial surveys. The proposed side scan array addresses concerns of acoustic survey inefficiency or poor image quality raised by several previous studies (Sagawa et al., 2008 ; Sabol et al., 2002 ; Paul et al., 2011 ; Lefebvre et al., 2009 ; DeFalco et al., 2010). This work demonstrates the ability of the constructed side scan array to survey seagrass habitat features accurately with an average over-estimation of feature area by 20.27% compared to satellite surveys and 13.15% compared to aerial surveys. These data are uncorrected for distortions, not adjusted for gain, and not corrected for vessel roll – all of which can be corrected to further improve accuracy. Functions for observed across-track and along-track distortion were calculated using known submerged objects and provided to encourage further corrections in similar future research. The array's high-resolution has also demonstrated promise for use in automated pattern recognition. It is our hope that both the utility and cost-efficiency of the proposed system will encourage seagrass and other coastal research in areas where cost may be a limiting factor or where traditional methods are not suitable due to shallow depth.

To the knowledge of the lead author parametric sonar has only been utilized once before in a seagrass environment by Lo Iacono et al., (2008), and this work represents the first study of its use in a shallow, non matte-forming seagrass environment. Parametric sonar has been introduced in this study as a potential method for remotely measuring the carbon content of seagrass sediments across large study sites. When compared to data from soil cores (n = 11), two reflectors observed in parametric readings (n = 31) taken over bare patches significantly associated with changes in soil porosity. Soil porosity showed no significant difference between vegetated and unvegetated sediments from depths 5 – 70 cm, indicating that Reflector 1 (MSD

24 cm) and Reflector 3 (MSD 56 cm) are likely to be present in the soil profile across both bare patches and the surrounding seagrass meadow (Fig. 35).

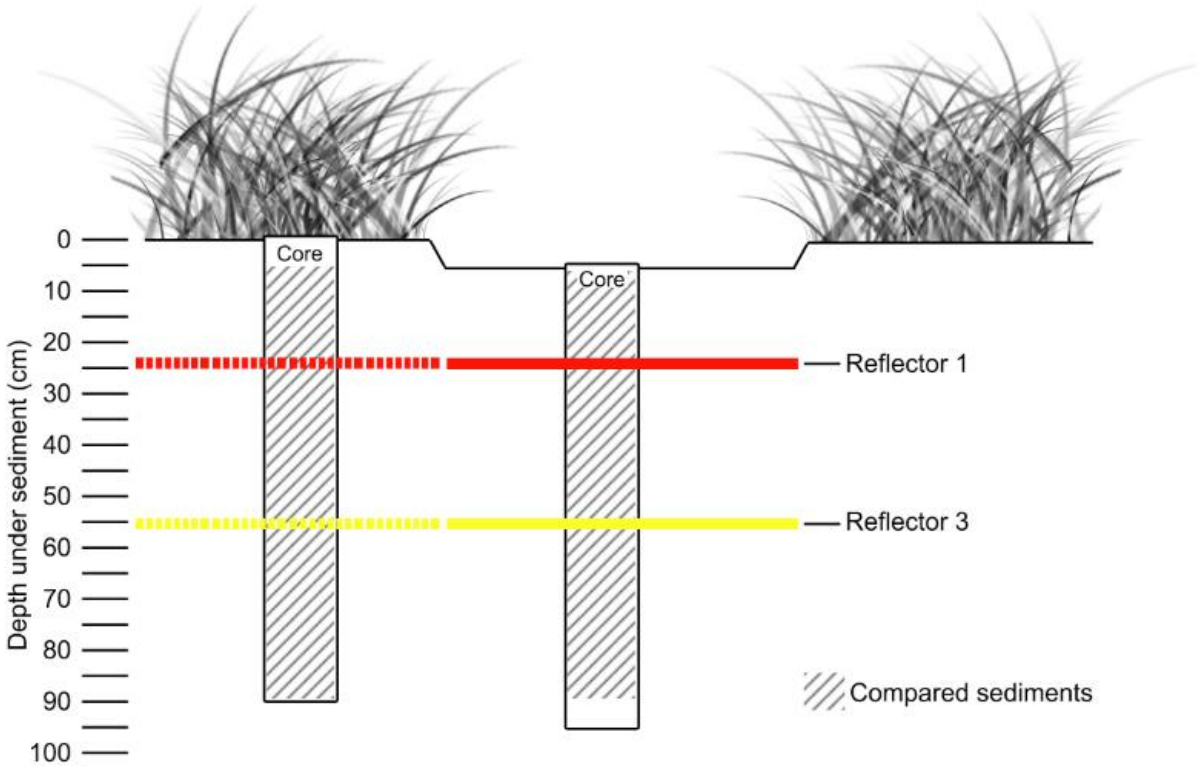

Figure 35, summary of mean depths for Reflector 1 and Reflector 3, and the proposed sediment layers in which they occur determined by the range of porosity-gradient maxima observed in soil core data. Similarity of porosity in the soil profiles of vegetated and unvegetated sediments suggest these reflectors can be inferred into seagrass meadows surrounding a sampled bare patch.

Lo Iacono et al., presented similar methods for the measurement of an entire seagrass matte derived from *Posidonia sp. (2008)*. This study expands the detection of layers in seagrass-enriched soils from simplified matte-forming systems to non-matt-forming species of seagrass such as *Thalassia testudinum* where organic carbon is stored in a complex, continuous soil matrix. This study has demonstrated that parametric sonar returns may be used in conjunction with a limited number of soil core to inform on the distributions of organic carbon across large spatial scales with complex habitat coverage. Reflectors associated with soil layers observed in

both vegetated and unvegetated sediments were shown to account for as much as 76% of the total organic carbon present in these areas to a depth of 90 cm. Software packages such as SonarWiz 6 also may allow for the incorporation of satellite, aerial, or acoustic surveys for seagrass coverage which expand modeling capabilities to include parameters for seagrass coverage or canopy height. Future research utilizing cores longer than 1 m may accomplish full rectification of all parametric reflectors occurring beyond the 90 cm scope of this paper which may be of interest in older bay systems than the one studied here. Evidence was also presented to indicate that parametric surveys conducted during seagrass' dormant period may yield considerably more recordings of seabed reflectors in vegetated areas, potentially reducing the degree of interpolation required between sample locations.

Over the course of this thesis we have presented systems for measuring both the above-ground coverage of seagrass meadows, and the below-ground carbon content of these systems. Our findings that cost-efficiency and availability of recreational side scan sonar components has reached a point where high-resolution mapping tools can be produced at minimal cost. These inexpensive arrays are robust and function well in an environment that is consistently understudied in mapping efforts of seagrass habitat coverage. Similarly, we have expanded on previous work by Lo Iacono et al., (2008) to demonstrate that parametric sonar is capable of discerning acoustic reflectors beneath sediments which were historically part of a large seagrass meadow. By concentrating parametric surveys over bare patches, which have remarkably similar soil characteristics to the surrounding seagrass meadow, remote measurements of carbon content may be taken of a large seagrass area using minimal soil coring as a reference for porosity-gradient and carbon content of these two sediment profiles. As a whole this thesis presents proof-of-concept for methods measuring two distinct metrics of seagrass ecosystems and encourages

their further development to benefit our understanding of how shallow coastal ecosystems function at large scales.

REFERENCES

Ardizzone, G., Belluscio, A., & Maiorano, L. (2006). Long-term change in the structure of a Posidonia oceanica landscape and its reference for a monitoring plan. *Marine Ecology*, 27(4), 299-309.

Avnimelech, Y., Ritvo, G., Meijer, L. E., & Kochba, M. (2001). Water content, organic carbon and dry bulk density in flooded sediments. Aquacultural engineering, 25(1), 25-33.

Bos, A. R., Bouma, T. J., de Kort, G. L., & van Katwijk, M. M. (2007). Ecosystem engineering by annual intertidal seagrass beds: sediment accretion and modification. *Estuarine, Coastal and Shelf Science*, 74(1), 344-348.

Blankenship, K. (2006). Underwater grasses at the tipping point?. *Bay Journal*, 16(6).

Bučas, M., Šaškov, A., Šiaulys, A., & Sinkevičienė, Z. (2016). Assessment of a simple hydroacoustic system for the mapping of macrophytes in extremely shallow and turbid lagoon. *Aquatic Botany*, 134, 39-46.

Bouillon, S., Borges, A. V., Castañeda-Moya, E., Diele, K., Dittmar, T., Duke, N. C., & Rivera-Monroy, V. H. (2008). Mangrove production and carbon sinks: a revision of global budget estimates. Global Biogeochemical Cycles, 22(2).

Dalal, R. C., & Henry, R. J. (1986). Simultaneous determination of moisture, organic carbon, and total nitrogen by near infrared reflectance spectrophotometry. Soil Science Society of America Journal, 50(1), 120-123.

De Falco, G., Tonielli, R., Di Martino, G., Innangi, S., Simeone, S., & Parnum, I. M. (2010). Relationships between multibeam backscatter, sediment grain size and Posidonia oceanica seagrass distribution. Continental Shelf Research, 30(18), 1941-1950.

Dekker, A. G., Anstee, J. M., & Brando, V. E. (2003). Seagrass change assessment using satellite data for Wallis Lake, NSW. CSIRO Land and Water, Technical Report.

Donato, D. C., Kauffman, J. B., Murdiyarso, D., Kurnianto, S., Stidham, M., & Kanninen, M. (2011). Mangroves among the most carbon-rich forests in the tropics. Nature Geoscience, 4(5), 293-297.

Duarte, C. M., Middelburg, J. J., & Caraco, N. (2005). Major role of marine vegetation on the oceanic carbon cycle. Biogeosciences, 2(1), 1-8.

Duarte, C. M., Marbà, N., Gacia, E., Fourqurean, J. W., Beggins, J., Barrón, C., & Apostolaki, E. T. (2010). Seagrass community metabolism: Assessing the carbon sink capacity of seagrass meadows. Global Biogeochemical Cycles, 24(4).

Dunton, K. H., & Schonberg, S. V. (2002). Assessment of propeller scarring in seagrass beds of the south Texas coast. *Journal of Coastal Research*, 100-110.

FAA. (2016). Public Law 114-90, Title II, Subtitle B – UAS Safety (FAA Extension, Safety, and Security Act of 2016). Accessed 12 February 2017 via: https://www.faa.gov/uas/resources/uas_regulations_policy/

Fourqurean, J. W., Kendrick, G. A., Collins, L. S., Chambers, R. M., & Vanderklift, M. A. (2012). Carbon, nitrogen and phosphorus storage in subtropical seagrass meadows: examples from Florida Bay and Shark Bay. Marine and Freshwater Research, 63(11), 967-983.

Fourqurean, J. W., Willsie, A., Rose, C. D., & Rutten, L. M. (2001). Spatial and temporal pattern in seagrass community composition and productivity in south Florida. *Marine Biology*, *138*(2), 341-354.

Fourqurean, J. W., Duarte, C. M., Kennedy, H., Marbà, N., Holmer, M., Mateo, M. A. & Serrano, O. (2012). Seagrass ecosystems as a globally significant carbon stock. *Nature geoscience*, 5(7), 505-509.

Fourqurean, J. W., & Zieman, J. C. (1991). Photosynthesis, respiration and whole plant carbon budget of the seagrass *Thalassia testudinum*. *Marine ecology progress series*. Oldendorf, 69(1), 161-170.

Gerlotto, F., Soria, M., & Fréon, P. (1999). From two dimensions to three: the use of multibeam sonar for a new approach in fisheries acoustics. *Canadian Journal of Fisheries and Aquatic Sciences*, 56(1), 6-12.

Gomez, C., Rossel, R. A. V., & McBratney, A. B. (2008). Soil organic carbon prediction by hyperspectral remote sensing and field vis-NIR spectroscopy: An Australian case study. Geoderma, 146(3), 403-411.

Howard, J., Hoyt, S., Isensee, K., Telszewski, M., Pidgeon, E. (2014) Coastal Blue Carbon: Methods for assessing carbon stocks and emissions factors in mangroves, tidal salt marshes, and seagrasses. Conservation International, Intergovernmental Oceanographic

Commission of UNESCO, International Union for Conservation of Nature. Arlington, Virginia, USA.

IPCC (2007). Contribution of working groups I, II and III to the fourth assessment report of the intergovernmental panel on climate change. IPCC, Geneva, Switzerland, 104.

Jordan, A., Lawler, M., Halley, V., & Barrett, N. (2005). Seabed habitat mapping in the Kent Group of islands and its role in marine protected area planning. Aquatic Conservation: Marine and Freshwater Ecosystems, 15(1), 51-70.

Kaeser, A. J., & Litts, T. L. (2010). A novel technique for mapping habitat in navigable streams using low-cost side scan sonar. *Fisheries*, 35(4), 163-174.

Karpouzli, E., & Malthus, T. J. (2007). Integrating dual frequency side scan sonar and high spatial resolution satellite imagery for monitoring coral reef benthic communities. *Geoscience and Remote Sensing Symposium*, 2007. IGARSS 2007. IEEE International (pp. 1730-1733). IEEE.

Kennedy, H., Beggins, J., Duarte, C. M., Fourqurean, J. W., Holmer, M., Marbà, N., & Middelburg, J. J. (2010). Seagrass sediments as a global carbon sink: isotopic constraints. Global Biogeochemical Cycles, 24(4).

Kenny, A. J., Cato, I., Desprez, M., Fader, G., Schüttenhelm, R. T. E., & Side, J. (2003). An overview of seabed-mapping technologies in the context of marine habitat classification. ICES *Journal of Marine Science: Journal du Conseil*, 60(2), 411-418.

Key, W. H. (2000). Side scan sonar technology. In OCEANS 2000 MTS/IEEE Conference and Exhibition (Vol. 2, pp. 1029-1033). IEEE.

Komatsu, T., Igarashi, C., Tatsukawa, K., Sultana, S., Matsuoka, Y., & Harada, S. (2003). Use of multi-beam sonar to map seagrass beds in Otsuchi Bay on the Sanriku Coast of Japan. *Aquatic Living Resources*,*16*(3), 223-230.

Lavery, P.S., Mateo, M.A., Serrano, O., & Rozaimi, M. (2013) Variability in the carbon storage of seagrass habitats and its implications for global estimates of blue carbon ecosystem service. *PloS one*, 8(9), e73748.

Lee, K. S., & Dunton, K. H. (1996). Production and carbon reserve dynamics of the seagrass *Thalassia testudinum* in Corpus Christi Bay, Texas, USA. *Marine Ecology Progress Series*, 143, 201-210.

Lee, K. M., Ballard, M. S., McNeese, A. R., & Wilson, P. S. (2017). Sound speed and attenuation measurements within a seagrass meadow from the water column into the seabed. *The Journal of the Acoustical Society of America*, 141(4), EL402-EL406.

Le Bas, T.P., Huvenne, V.A.I. (2009). Acquisition and processing of backscatter data for habitat mapping – Comparison of multibeam and sidescan systems. *Applied Acoustics*, 70, 1248-1257.

Lefebvre, A., Thompson, C. E. L., Collins, K. J., & Amos, C. L. (2009). Use of a high-resolution profiling sonar and a towed video camera to map a Zostera marina bed, Solent, UK. *Estuarine, Coastal and Shelf Science*, *82*(2), 323-334.

Lo Iacono, C., Mateo, M. A., Gracia, E., Guasch, L., Carbonell, R., Serrano, L., & Danobeitia, J. (2008). Very high-resolution seismo-acoustic imaging of seagrass meadows (Mediterranean Sea): Implications for carbon sink estimates. *Geophysical Research Letters*, *35*(18).

Lucieer, V. L. (2008). Object-oriented classification of sidescan sonar data for mapping benthic marine habitats. *International Journal of Remote Sensing*, 29(3), 905-921.

Luo, X., Wang, Y., & Luczhovich, J. (2016, July). Mapping submerged aquatic vegetation in albemarle sound, NOrth Carolina, USA using Landsat-8 and SONAR data. *Geoscience and Remote Sensing Symposium* (IGARSS), 2016 IEEE International (pp. 3802-3805). IEEE.

Lurton, X. (2002). *An introduction to underwater acoustics: principles and applications*. Springer Science & Business Media.

Macreadie, P. I., Baird, M. E., Trevathan-Tackett, S. M., Larkum, A. W. D., & Ralph, P. J. (2014). Quantifying and modelling the carbon sequestration capacity of seagrass meadows–a critical assessment. Marine pollution bulletin, 83(2), 430-439.

Majer, J. D., Delabie, J. H. C., & McKenzie, N. L. (1997). Ant litter fauna of forest, forest edges and adjacent grassland in the Atlantic rain forest region of Bahia, Brazil. *Insectes Sociaux*, 44(3), 255-266.

Mazel, C. (1985). *Side scan sonar record interpretation.* Klein Associates Inc.

Mcleod, E., Chmura, G. L., Bouillon, S., Salm, R., Björk, M., Duarte, C. M., & Silliman, B. R. (2011). A blueprint for blue carbon: toward an improved understanding of the role of vegetated coastal habitats in sequestering CO2. Frontiers in Ecology and the Environment, 9(10), 552-560.

Micallef, A., Le Bas, T. P., Huvenne, V. A., Blondel, P., Hühnerbach, V., & Deidun, A. (2012). A multi-method approach for benthic habitat mapping of shallow coastal areas with high-resolution multibeam data. Continental Shelf Research, 39, 14-26.

Mulhearn, P. J. (2001). *Mapping seabed vegetation with sidescan sonar* (No. DSTO-TN-0381). Defense Science and Technology Organization Victoria (Australia). Aeronautical and Maritime Research Lab.

Mumby, P. J., Green, E. P., Edwards, A. J., & Clark, C. D. (1999). The cost-effectiveness of remote sensing for tropical coastal resources assessment and management. *Journal of Environmental Management*, *55*(3), 157-166.

Munday, E., Moore, B., & Burczynski, J. (2013, September). Hydroacoustic mapping system for quantitative identification of aquatic macrophytes, substrate composition, and shallow water bathymetric surveying. In Oceans-San Diego, 2013 (pp. 1-3). IEEE.

Murray, B. C., Pendleton, L., Jenkins, W. A., & Sifleet, S. (2011). Green payments for blue carbon: Economic incentives for protecting threatened coastal habitats. Nicholas Institute for Environmental Policy Solutions, Report NI, 11(04).

Norris, J. G., Wyllie-Echeverria, S., Mumford, T., Bailey, A., & Turner, T. (1997). Estimating basal area coverage of subtidal seagrass beds using underwater videography. *Aquatic Botany*, *58*(3), 269-287.

Oelze, M. L., O'Brien, W. D., & Darmody, R. G. (2002). Measurement of attenuation and speed of sound in soils. Soil Science Society of America Journal, 66(3), 788-796.

Orth, R. J., Carruthers, T. J., Dennison, W. C., Duarte, C. M., Fourqurean, J. W., Heck Jr, K. L., & Short, F. T. (2006). A global crisis for seagrass ecosystems. *Bioscience*, 56(12), 987-996.

Paul, M., Lefebvre, A., Manca, E., & Amos, C. L. (2011). An acoustic method for the remote measurement of seagrass metrics. *Estuarine, Coastal and Shelf Science*, 93(1), 68-79.

Pasqualini, V., Pergent-Martini, C., Clabaut, P., & Pergent, G. (1998). Mapping of Posidonia Oceanica using Aerial Photographs and Side Scan Sonar: Application off the Island of Corsica (France). *Estuarine, Coastal and Shelf Science*, 47(3), 359-367.

Pasqualini, V., Pergent-Martini, C., & Pergent, G. (1999). Environmental impact identification along the Corsican coast (Mediterranean Sea) using image processing. *Aquatic Botany*, 65(1), 311-320.

Pasqualini, V., Clabaut, P., Pergent, G., Benyoussef, L., & Pergent-Martini, C. (2000). Contribution of side scan sonar to the management of Mediterranean littoral ecosystems. *International Journal of Remote Sensing*, 21(2), 367-378.

Pendleton, L., Donato, D. C., Murray, B. C., Crooks, S., Jenkins, W. A., Sifleet, S., & Megonigal, P. (2012). Estimating global "blue carbon" emissions from conversion and degradation of vegetated coastal ecosystems. PloS one, 7(9), e43542.

Pergent, G., Romero, J., Pergent-Martini, C., Mateo, M. A., & Boudouresque, C. F. (1994). Primary production, stocks and fluxes in the Mediterranean seagrass Posidonia oceanica. Marine Ecology-Progress Series, 106, 139-139.

Pergent, G., Bazairi, H., Bianchi, C. N., Boudouresque, C. F., Buia, M. C., Calvo, S., & Morri, C. (2014). Climate change and Mediterranean seagrass meadows: a synopsis for environmental managers. Mediterranean Marine Science, 15(2), 462-473.

Pergent, G., Pergent-Martini, C., De Florinier, M., Bonacorsi, M., Clabaut, P., & Valette-Sansevin, A. (2015). Assessment of carbon sequestrated within the matte of the Posidonia oceanica meadow at the NATURA 2000 site "Grand Herbier de la Plaine Orientale" (No. e1378). PeerJ PrePrints.

Phinn, S., Roelfsema, C., Dekker, A., Brando, V., & Anstee, J. (2008). Mapping seagrass species, cover and biomass in shallow waters: An assessment of satellite multi-spectral and airborne hyper-spectral imaging systems in Moreton Bay (Australia). *Remote Sensing of Environment,112*(8), 3413-3425

Rahnemoonfar, M., Ashapure, A., Rahman A., Kline R., & Greene A. (2016). Automatic seagrass disturbance pattern identification on sonar images. *In Review*.

Ramakrishnan, N. (1994). Speed of sound in porous materials. Bulletin of Materials Science, 17(5), 499-504.

Riegl, B., Moyer, R. P., Morris, L., Virnstein, R., & Dodge, R. E. (2005). Determination of the distribution of shallow-water seagrass and drift algae communities with acoustic seafloor discrimination. *Revista de biología tropical, 53*, 165-174.

Ritter, N., Ruth M. (2000). GeoTIFF format specification (GeoTIFF revision 1.0). Accessed December 2016. URL: http://web.archive.org/web/20160403164508/http://www.remotesensing.org/geotiff/spec/geotiffhome.html.

Sabol, B. M., Eddie Melton, R., Chamberlain, R., Doering, P., & Haunert, K. (2002). Evaluation of a digital echo sounder system for detection of submersed aquatic vegetation. *Estuaries and Coasts*, 25(1), 133-141.

Sagawa, T., Mikami, A., Komatsu, T., Kosaka, N., Kosako, A., Miyazaki, S., & Takahashi, M. (2008). Technical Note. Mapping seagrass beds using IKONOS satellite image and side scan sonar measurements: a Japanese case study. *International Journal of Remote Sensing*, 29(1), 281-291.

Sánchez-Carnero, N., Rodríguez-Pérez, D., Couñago, E., Aceña, S., & Freire, J. (2012). Using vertical Sidescan Sonar as a tool for seagrass cartography. *Estuarine, Coastal and Shelf Science*, 115, 334-344.

Serrano, O., Lavery, P. S., Rozaimi, M., & Mateo, M. Á. (2014). Influence of water depth on the carbon sequestration capacity of seagrasses. Global Biogeochemical Cycles, 28(9), 950-961.

Tunnell, J. W., & Judd, F. W. (2002). The Laguna Madre of Texas and Tamaulipas (Vol. 2). Texas A&M University Press.

Uhrin, A. V., & Holmquist, J. G. (2003). Effects of propeller scarring on macrofaunal use of the seagrass *Thalassia testudinum*. *Marine Ecology Progress Series*, 250, 61-70.

Warren, J. D., & Peterson, B. J. (2007). Use of a 600-kHz Acoustic Doppler Current Profiler to measure estuarine bottom type, relative abundance of submerged aquatic vegetation, and eelgrass canopy height. Estuarine, Coastal and Shelf Science, 72(1), 53-62.

Waycott M., Duarte C.M., Carruthers T., Orth R.J., Dennison W., Olyarnik S., Calladine A., Fourqurean J.W., Heck K.L., Hughes R.A., Kendrick G.A., Kenworthy J.W., Short F.T., Williams S.L., "Accelerating loss of seagrasses across the globe threatens coastal ecosystems." *PNAS* 2009 106 (30) 12377-12381; doi:10.1073/pnas.0905620106

Wilcox, B. A., & Murphy, D. D. (1985). Conservation strategy: the effects of fragmentation on extinction. *The American Naturalist*, 125(6), 879-887.

Wilson, C. J., Wilson, P. S., Greene, C. A., & Dunton, K. H. (2013). Seagrass meadows provide an acoustic refuge for estuarine fish. *Marine Ecology Progress Series*, 472, 117-127.

Wilson P.S., and Dunton K.H., "Laboratory investigation of the acoustic response of seagrass tissue in the frequency band 0.5–2.5 kHz," J. *Acoust. Soc. Am.* 125, 1951–1959 (2009).

Wilson P.S., Reed A.H., Wood W.T., and Roy R.A., "Low frequency sound speed measurements paired with computed x-ray tomography imaging in gas-bearing reconstituted natural sediments," in *Proceedings of the 2nd International Conference and Exhibition on Underwater Acoustics Measurements: Technologies and Results*, J. S. Papadakis and L. Bjørnø, Eds. Heraklion, Greece, 2007, pp. 21–29, ISBN 978-960-88702-5-3.

Wilson P.S., Reed A.H., Wood W.T., and Roy R.A., "The low-frequency sound speed of fluid-like gas-bearing sediments," *J. Acoust. Soc. Am.* 123, EL99–EL104 (2008)

Wunderlich, J., Wendt, G., & Müller, S. (2005). High-resolution echo-sounding and detection of embedded archaeological objects with nonlinear sub-bottom profilers. Marine Geophysical Researches, 26(2-4), 123-133.

Zieman, J. C. (1974). Methods for the study of the growth and production of turtle grass, *Thalassia testudinum*. König. *Aquaculture*, 4, 139-143.

Zieman, J.C. (1976). The ecological effects of physical damage from motorboats on turtle grass beds in southern Florida. *Aquatic Botany*, 2, 127-139.

APPENDIX A

APPENDIX A

ESTIMATED COSTS OF COMMERCIALLY AVAILABLE SIDE SCAN FOR USE IN SHALLOW WATER

Brand	Manufacturer Recommended Unit	Frequency	Cost
EdgeTech	4125 Side Scan	400/900 kHz	~$45,000
Marine Sonic Technology	ARC Explorer CHIRP Side Scan	1800 kHz	~$39,000
Kongsberg	PulSAR Side Scan	550-1000 kHz	~$30,000
JW Fisher	SSS-1200K Side Scan	1200 kHz	~$21,000
TriTech Co.	StarFish 990F Side Scan	990 kHz	~$7,379
	Lab Created Unit	**455/800 kHz**	**~$1,740**

APPENDIX B

APPENDIX B

DEMONSTRATION OF SSS-OBSERVED FEATURES IN A SHALLOW SEAGRASS BED. SHOWN WITH ADDITIONAL PROCESSING FOR GAIN AND BEAM ANGLE CORRECTION PERFORMED IN SONARWIZ 6

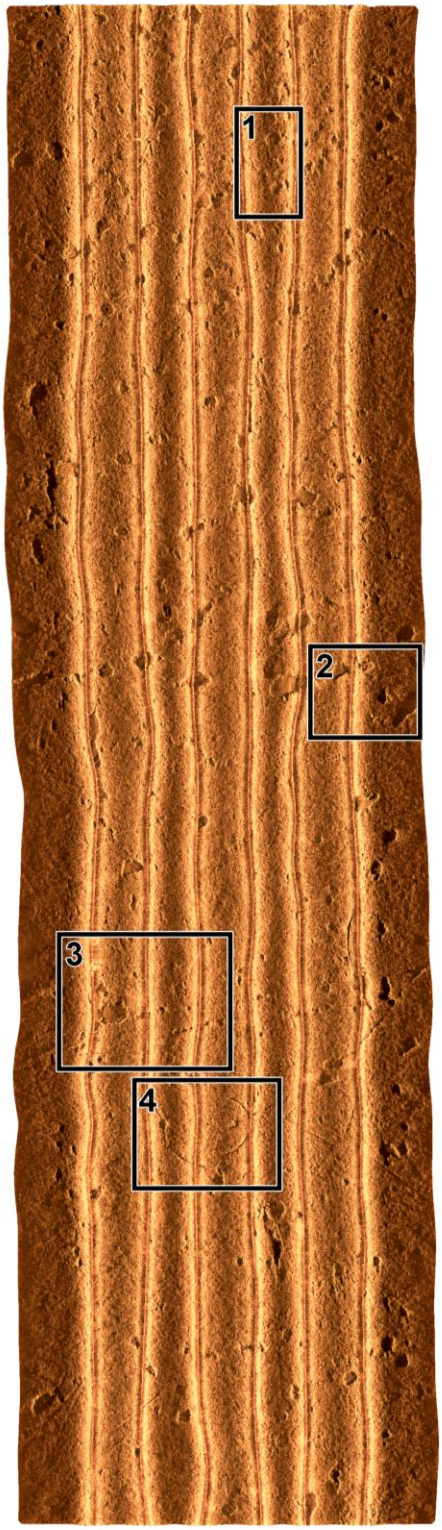

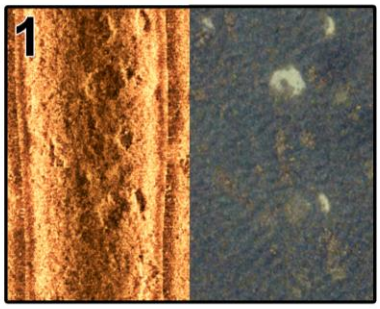

Same area shown in both side scan and drone imagery. Bare patches which have been filled with drift algae are difficult to spot in drone imagery, but clearly visible in side scan.

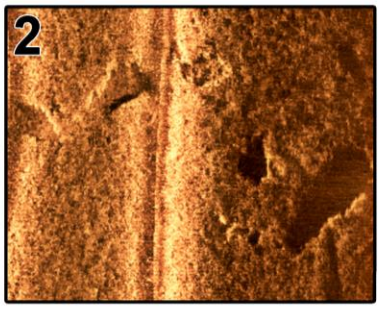

Bare patches are clearly represented in side scan imagery throughout the horizontal range. In this sample features can be clearly seen from 0 - 25 m from the transducer.

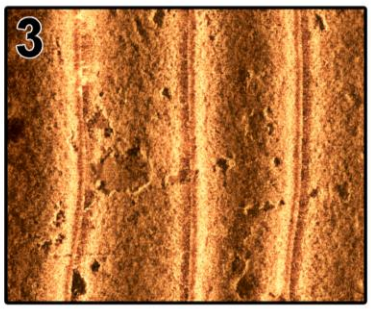

Features of a variety of sizes are visible. In this area bare patches up to 56 m^2 are visible as well as small features < 3 m^2.

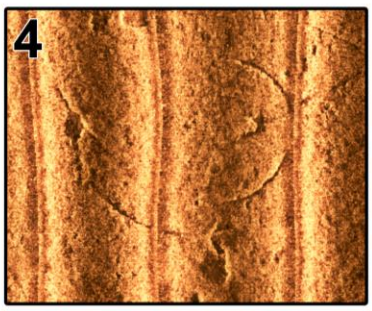

Indicators of anthropogenic disturbance are visible as well throughout the study site, such as this area with multiple propeller scars.

APPENDIX C

APPENDIX C

DEMONSTRATION OF SSS-OBSERVED FEATURES DETECTED VIA AUTOMATIC PATTERN RECOGNITION PROCESSES (Rahnemoonfar et al., 2016, in review)

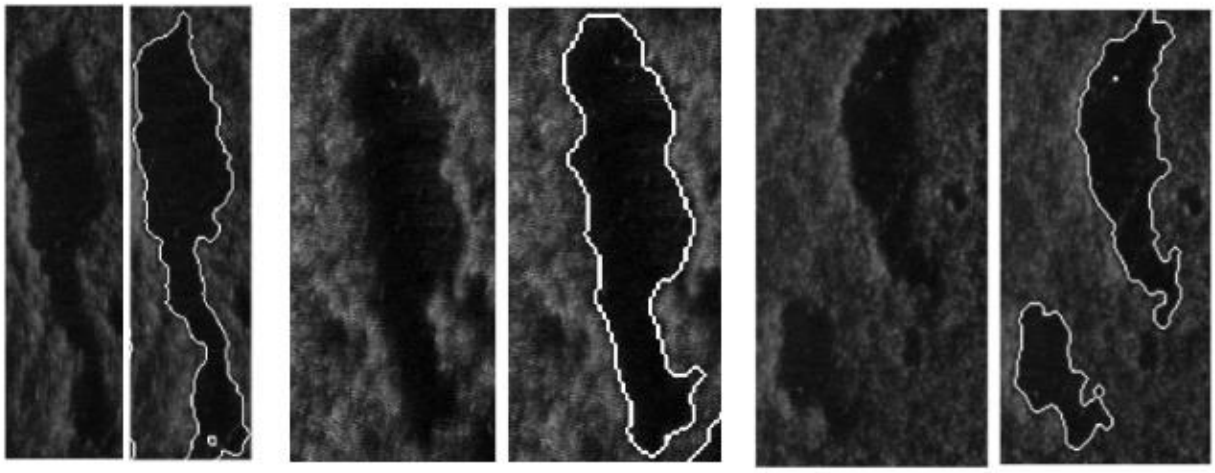

APPENDIX D

APPENDIX D

SOFTWARE PACKAGES USED AND THEIR SOURCE

Software Title	Manufacturer Website
ArcMap 10.3	www.desktop.arcgis.com
SonarWiz 6	www.chesapeaketech.com/products/sonarwiz-sidescan
SonarTRX	www.sonartrx.com
Innomar IDE	www.innomar.com
Innomar SES	www.innomar.com

APPENDIX E

APPENDIX E

MAP OF SIDE SCAN SONAR TRANSECT LINES

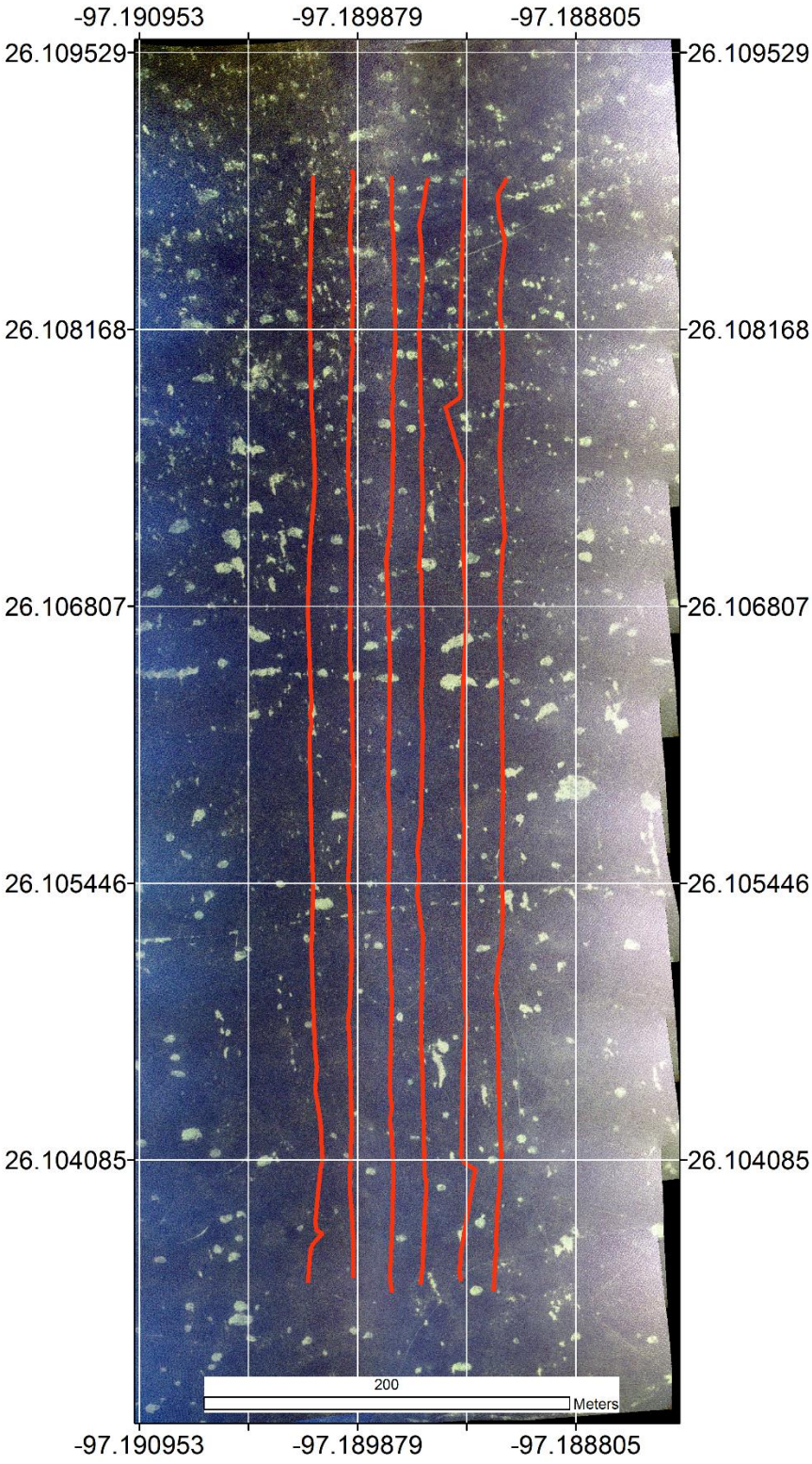
-97.190953
-97.189879
-97.188805
26.109529
26.108168
26.106807
26.105446
26.104085
200
Meters

APPENDIX F

APPENDIX F

MAP OF PARAMETRIC SONAR TRANSECT LINES

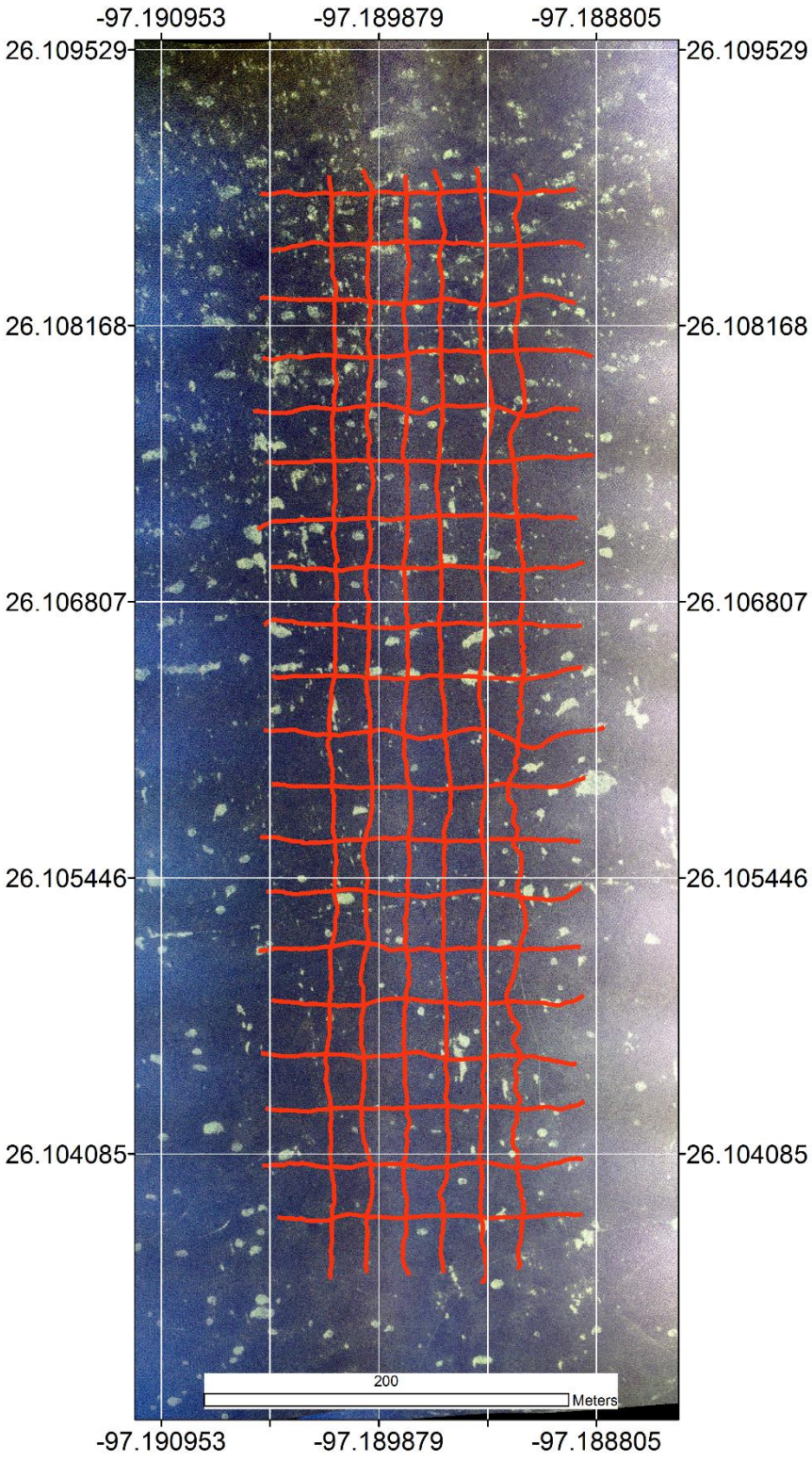
-97.190953
-97.189879
-97.188805
26.109529
26.108168
26.106807
26.105446
26.104085
200
Meters

APPENDIX G

APPENDIX G

SCHEMATIC OF SIDE SCAN SONAR ARRAY

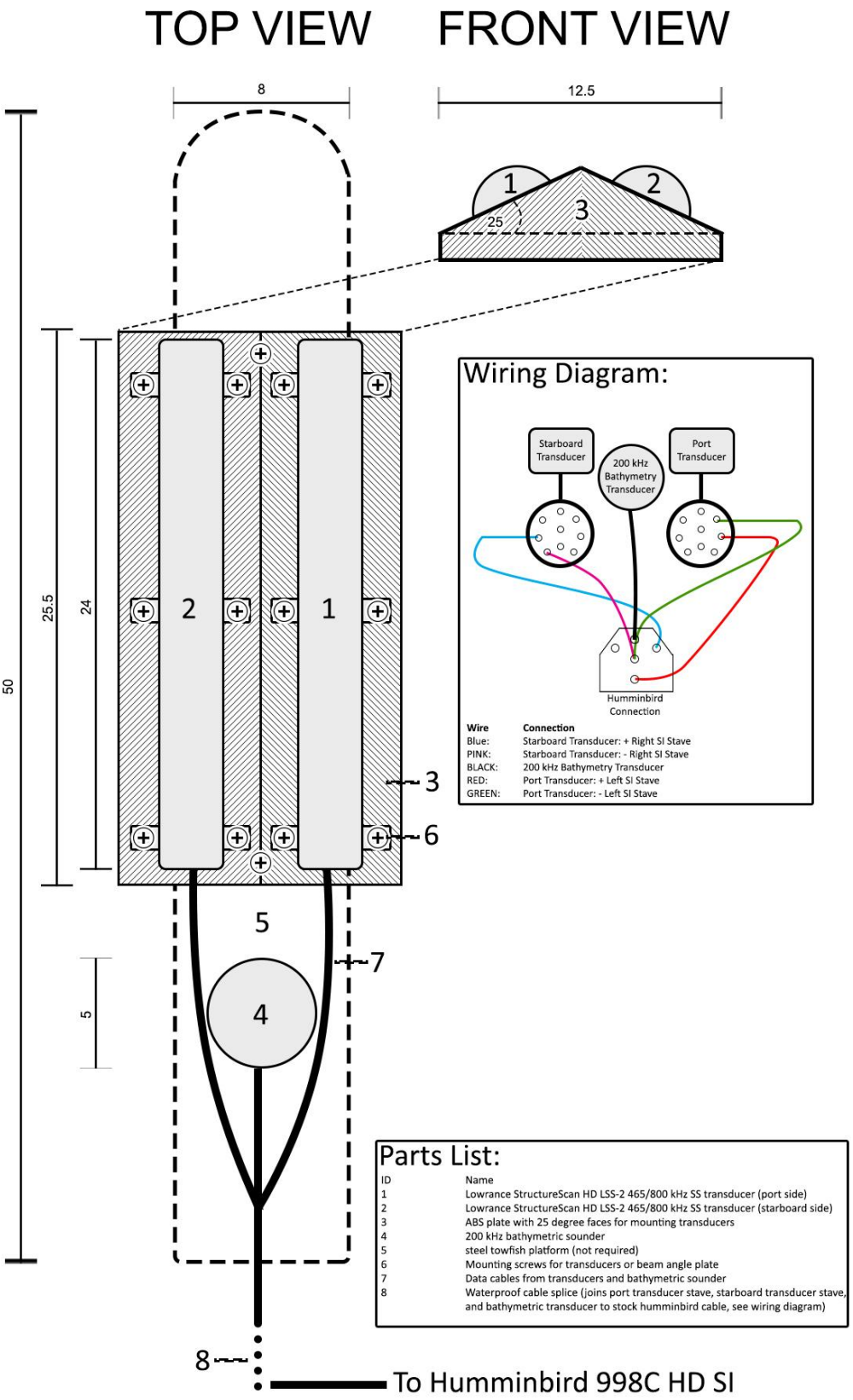

Parts List:

ID	Name
1	Lowrance StructureScan HD LSS-2 465/800 kHz SS transducer (port side)
2	Lowrance StructureScan HD LSS-2 465/800 kHz SS transducer (starboard side)
3	ABS plate with 25 degree faces for mounting transducers
4	200 kHz bathymetric sounder
5	steel towfish platform (not required)
6	Mounting screws for transducers or beam angle plate
7	Data cables from transducers and bathymetric sounder
8	Waterproof cable splice (joins port transducer stave, starboard transducer stave, and bathymetric transducer to stock humminbird cable, see wiring diagram)

BIOGRAPHICAL SKETCH

Austin L. Greene attended the University of California, Davis and earned a bachelor's of science in Evolution, Ecology & Biodiversity in June 2014. During his undergraduate career Austin contributed to studies ranging from intertidal community structure, entomological diversity, to the political sciences, and was awarded the Provost' Undergraduate Research Fellowship in December 2014. After graduating Austin conducted field work in South Korea under Dr. Kun-Seop Lee as part of the Zostera Experimental Network (ZEN) seagrass monitoring project. In August 2015 Austin began his masters thesis under Dr. Abdullah Faiz Rahman at the University of Texas, Rio Grande Valley which he completed in May 2017. Austin has been accepted into a doctoral position at the University of Hawaii, Manoa under Dr. Megan Donahue. Starting in Fall 2017 he will continue his career in research by studying the impacts and distribution of disease on coral reefs.